

Chapter 3

Past plate motions

3.1 The role of the Earth's magnetic field

3.1.1 Introduction

It should be clear from the preceding chapter that it is possible, without too much difficulty, to calculate the relative motions of pairs of plates at any location along their common boundary and to see what may occur in the future. This chapter deals with the past motions of the plates and shows how to reconstruct their previous interactions from evidence they have left.

Two important facts together make it possible to determine past plate motions. The first is that the Earth's magnetic field has not always had its present (normal) polarity with the 'north' magnetic pole close to the north geographic pole¹ and the 'south' magnetic pole close to the south geographic pole. Over geological history the magnetic field has intermittently reversed. Thus, there have been times in the past when the north magnetic pole has been located close to the present-day south geographic pole and the south magnetic pole has been located close to the present-day north geographic pole; then the field is said to be reversed. The second fact is that, under certain circumstances (discussed in Section 3.2) rocks can record the Earth's past (*palaeo*) magnetic field. Together, these facts enable us to estimate dates and past positions of the plates from magnetic measurements.

3.1.2 The Earth's magnetic field

To specify the geomagnetic field at any point on the Earth's surface both a magnitude and a direction are required: the geomagnetic field is a vector quantity. It is far from being constant either in magnitude or in direction and varies spatially over the surface of the Earth as well as in time. Systematic mapping of the magnetic field began some five hundred years ago with the magnetic compass measurements carried out by the early mariners. The internationally agreed values of the geomagnetic field are updated and published every few years as the *International Geomagnetic Reference Field* (IGRF). Figure 3.1(a) shows the

¹ The geomagnetic pole at present situated in the northern hemisphere is in fact a south pole since it attracts the north poles of magnets (compass needles)! See Fig. 3.2.

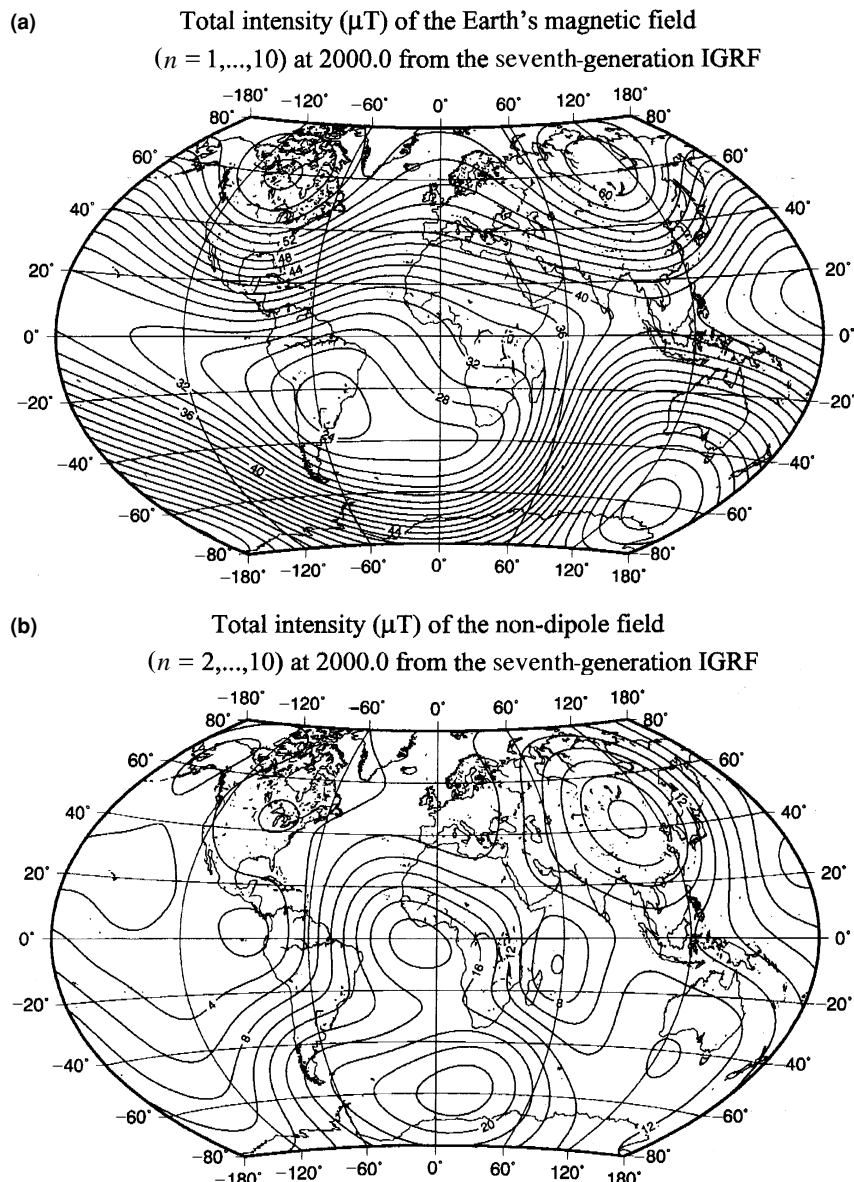


Figure 3.1. (a) The total intensity of the Earth's magnetic field in microteslas (μT).
(b) The total intensity of the non-dipole component of the Earth's magnetic field (magnetic field – best-fitting dipole field) in microteslas (μT). The field is the International Geomagnetic Reference Field (IGRF seventh generation). The nanotesla ($1 \text{ nT} = 10^{-3} \mu\text{T}$), an SI unit, is the same as gamma (γ), the magnetic field unit of the old c.g.s. system.

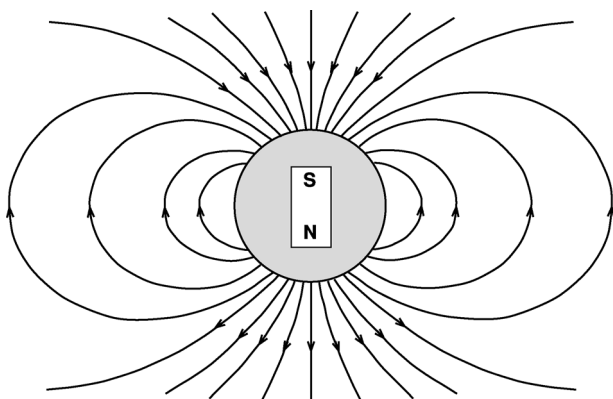


Figure 3.2. A magnetic dipole (e.g., a bar magnet) at the centre of the Earth has a magnetic field that is a good first approximation to the Earth's magnetic field. Note that the geomagnetic North Pole is so called because the north end of the compass needle points towards it (it is therefore actually a south magnetic pole). Such a dipole field would also be produced by a uniformly magnetized Earth, a uniformly magnetized core or particular current systems within the core (Fig. 8.23). The origin of the field and models of the core and possible reasons for the reversals of the Earth's magnetic field are discussed further in Section 8.3.2.

magnitude of the IGRF for 1995. To a first approximation the Earth's magnetic field is a *dipole field*.² This means that the Earth's magnetic field can be represented by a magnetic dipole situated at the centre of the Earth (imagine a bar magnet at the centre of the Earth, Fig. 3.2). This fact was first pointed out in 1600 by Sir William Gilbert.³ The difference between the Earth's magnetic field and the best dipole field is termed the *non-dipole field*. Figure 3.1(b) shows the magnitude of the non-dipole field. At the Earth's surface the non-dipole field is small compared with the dipole field, though this is not the case for the field at the core–mantle boundary.

Today, the best-fitting dipole is aligned at about 11.5° to the Earth's geographic north–south axis (spin axis). The geomagnetic poles are the two points where the axis of this best-fitting dipole intersects the Earth's surface. Now at 79°N , 71°W and 79°S , 109°E , they are called the *geomagnetic north* and *geomagnetic south poles*, respectively. The *geomagnetic equator* is the equator of the best-fitting dipole axis. The two points on the Earth's surface at which the magnetic field is vertical and has no horizontal component are called the *magnetic poles*, or *dip poles*. The present north magnetic pole is at 76°N , 101°W , and the south magnetic pole is at 66°S , 141°E . The *magnetic equator* is the line along which the magnetic field is horizontal and has no vertical component. If the field were

² The magnetic field produced by a bar magnet is a dipole field.

³ William Gilbert was a distinguished physician. He was President of the College of Physicians and physician to Queen Elizabeth I and King James I. His book *De Magnete* is in print in translation.

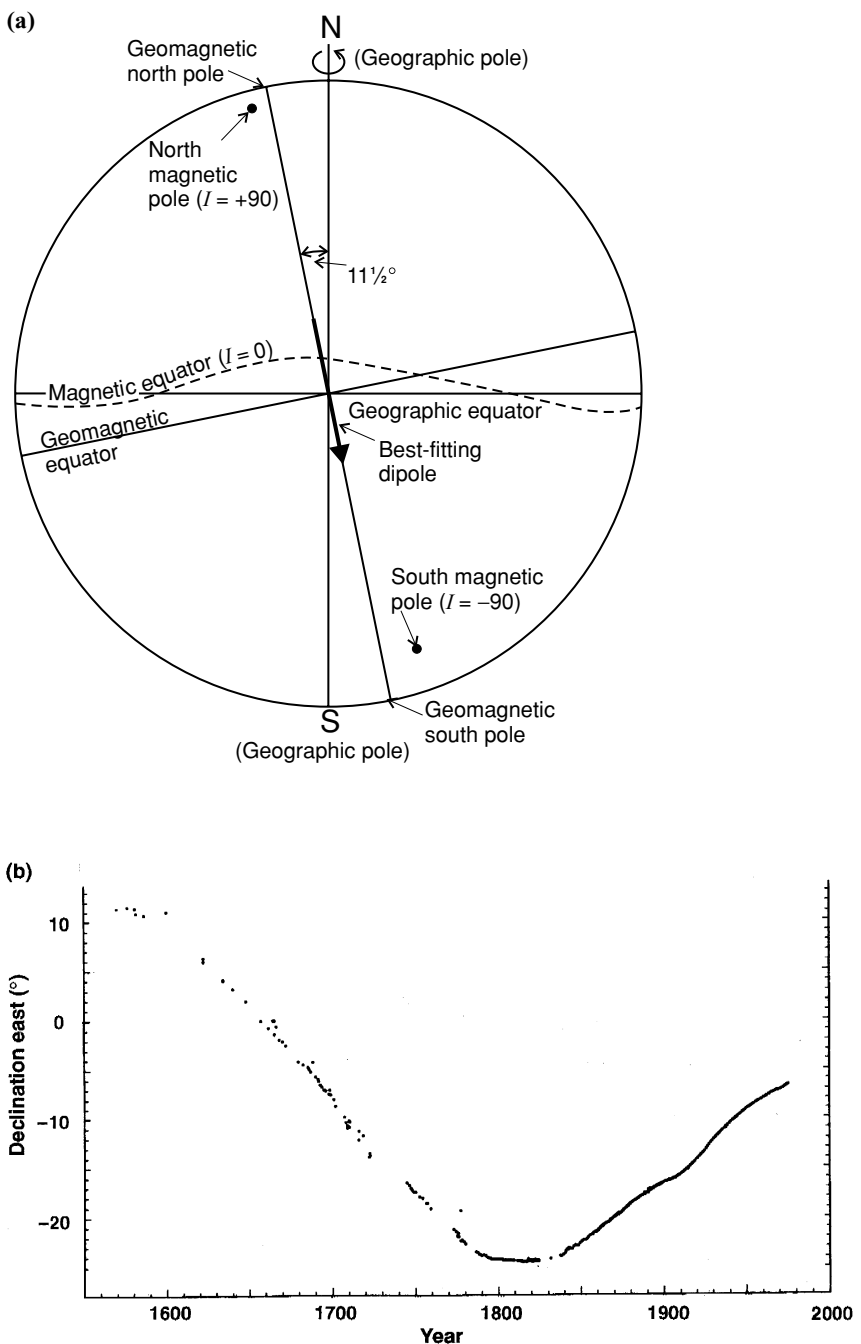


Figure 3.3. (a) A diagram illustrating the difference between the Earth's geographic, geomagnetic and magnetic poles and equator. (From McElhinny (1973).) (b) The change in magnetic declination as observed from London over four centuries. (From Malin and Bullard (1981).)

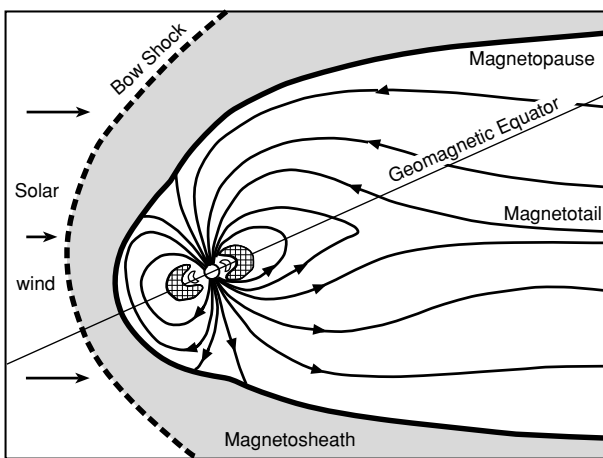


Figure 3.4. The Earth's magnetic field far from the Earth is controlled largely by the solar wind. The Van Allen radiation belts are the cross-hatched regions either side of the Earth. (After Hutton (1976).)

exactly a dipole field, these magnetic poles and this equator would be coincident with the geomagnetic north and south poles and equator. The various poles and equators are illustrated in Fig. 3.3.

Figure 3.4 shows the magnetic field lines around the Earth. The Sun plays the major part in the shape of the field far from the Earth and in the short-term variations of the field. The *solar wind*, a constant stream of ionized particles emitted by the Sun, confines the Earth's magnetic field to a region known as the *magnetosphere* and deforms the field lines so that the magnetosphere has a long 'tail', the *magnetotail*, which extends several million kilometres away from the Sun. A shock wave, the *bow shock*, is produced where the solar wind is slowed by interaction with the Earth's magnetic field. A turbulent zone within the bow shock is known as the *magnetosheath*, the inner boundary of which is called the *magnetopause*. The Earth's magnetic field shields the Earth from most of the incident radiation, and the atmosphere absorbs much of the remainder. Major sunspot activity causes changes in the solar wind, which in turn result in short-term fluctuations in the magnetic field known as *magnetic storms*. The *Van Allen radiation belts* are zones of charged particles trapped by the Earth's magnetic field. Any changes in the solar wind, and hence in the magnetic field, can allow these charged particles to enter the upper atmosphere, where they cause the spectacular auroral displays known as the *Northern* and *Southern Lights*. The active processes and interactions which take place between the magnetosphere and the solar wind are collectively referred to as 'space weather'. The Sun is also responsible for the *diurnal* (daily) variation in the Earth's magnetic field. This variation, which has an amplitude of less than 0.5% of the total field, is the main short-period variation in the Earth's magnetic field.

The long-term reversals of the magnetic field, mentioned in Section 3.1.1, are used to date the oceanic lithosphere. However, the geomagnetic field changes

on an intermediate timescale too: the pole wanders by a few degrees a century. This wandering has been measured throughout historical time and is termed *secular variation*. However, it appears that, on average over geological time, the geomagnetic field axis has been aligned along the Earth's spin axis (i.e., on average the geomagnetic poles have been coincident with the geographic poles). This means that, to a first approximation, the geomagnetic field can be modelled as the field of a dipole aligned along the geographic north–south axis. This assumption is critical to all palaeomagnetic work: if the dipole axis had wandered randomly in the past and had not, on average, been aligned along the geographic axis, all palaeomagnetic estimates of past positions of rock samples would be meaningless because they would be relative only to the position of the geomagnetic pole at the time each sample acquired its permanent magnetization and would have nothing at all to do with the geographic pole.

The *magnetic potential* from which the Earth's magnetic field is derived can be expressed as an infinite series of spherical harmonic functions. The first term in this series is the potential due to a dipole situated at the centre of the Earth. At any position \mathbf{r} , from a dipole, the magnetic potential $V(\mathbf{r})$ is given by

$$V(\mathbf{r}) = \frac{1}{4\pi r^3} \mathbf{m} \cdot \mathbf{r} \quad (3.1)$$

where \mathbf{m} is the dipole moment, a vector aligned along the dipole axis. For the Earth \mathbf{m} is $7.94 \times 10^{22} \text{ A m}^2$ in magnitude. The magnetic field $\mathbf{B}(\mathbf{r})$ at any position \mathbf{r} can then be determined by differentiating the magnetic potential:

$$\mathbf{B}(\mathbf{r}) = -\mu_0 \nabla V(\mathbf{r}) \quad (3.2)$$

where $\mu_0 = 4\pi \times 10^{-7} \text{ kg m A}^{-2} \text{ s}^{-2}$ is the magnetic permeability of free space (A is the abbreviation for amp).

To apply Eq. (3.2) to the Earth, we find it most convenient to work in spherical polar coordinates (r, θ, ϕ) , (r is the radius, θ the colatitude and ϕ the longitude or azimuth on the sphere, as shown in Fig. A1.4). The magnetic field $\mathbf{B}(\mathbf{r})$ is then written as $\mathbf{B}(\mathbf{r}) = (B_r, B_\theta, B_\phi)$ in this coordinate system. B_r is the radial component of the field, B_θ is the southerly component and B_ϕ is the easterly component. (See Appendix 1 for details of this and other coordinate systems.)

In spherical polar coordinates, if we assume that \mathbf{m} is aligned along the *negative* z axis (see caption for Fig. 3.2), Eq. (3.1) is

$$\begin{aligned} V(\mathbf{r}) &= \frac{1}{4\pi r^3} \mathbf{m} \cdot \mathbf{r} \\ &= -\frac{mr \cos \theta}{4\pi r^3} \\ &= -\frac{m \cos \theta}{4\pi r^2} \end{aligned} \quad (3.3)$$

Substitution of Eq. (3.3) into Eq. (3.2) gives the three components (B_r, B_θ, B_ϕ) of the magnetic field due to a dipole at the centre of the Earth. The radial component

of the field is B_r :

$$\begin{aligned} B_r(r, \theta, \phi) &= -\mu_0 \frac{\partial V}{\partial r} \\ &= \frac{\mu_0 m \cos \theta}{4\pi} \frac{\partial}{\partial r} \left(\frac{1}{r^2} \right) \\ &= -\frac{2\mu_0 m \cos \theta}{4\pi r^3} \end{aligned} \quad (3.4)$$

The component of the field in the θ direction is B_θ :

$$\begin{aligned} B_\theta(r, \theta, \phi) &= -\mu_0 \frac{1}{r} \frac{\partial V}{\partial \theta} \\ &= \frac{\mu_0 m}{4\pi r^3} \frac{\partial}{\partial \theta} (\cos \theta) \\ &= -\frac{\mu_0 m \sin \theta}{4\pi r^3} \end{aligned} \quad (3.5)$$

The third component is B_ϕ :

$$\begin{aligned} B_\phi(r, \theta, \phi) &= -\mu_0 \frac{1}{r \sin \theta} \frac{\partial V}{\partial \phi} \\ &= 0 \end{aligned} \quad (3.6)$$

Note that, by symmetry, there can obviously be no field in the ϕ (east) direction. The total field strength at any point is

$$\begin{aligned} B(r, \theta, \phi) &= \sqrt{B_r^2 + B_\theta^2 + B_\phi^2} \\ &= \frac{\mu_0 m}{4\pi r^3} \sqrt{1 + 3 \cos^2 \theta} \end{aligned} \quad (3.7)$$

Along the north-polar axis ($\theta = 0$) the field is

$$\begin{aligned} B_r(r, 0, \phi) &= -\frac{\mu_0 m}{2\pi r^3} \\ B_\theta(r, 0, \phi) &= 0 \end{aligned} \quad (3.8)$$

On the equator ($\theta = 90^\circ$) the field is

$$\begin{aligned} B_r(r, 90, \phi) &= 0 \\ B_\theta(r, 90, \phi) &= -\frac{\mu_0 m}{4\pi r^3} \end{aligned} \quad (3.9)$$

and along the south-polar axis ($\theta = 180^\circ$) the field is

$$\begin{aligned} B_r(r, 180, \phi) &= \frac{\mu_0 m}{2\pi r^3} \\ B_\theta(r, 180, \phi) &= 0 \end{aligned} \quad (3.10)$$

If we define a constant B_0 as

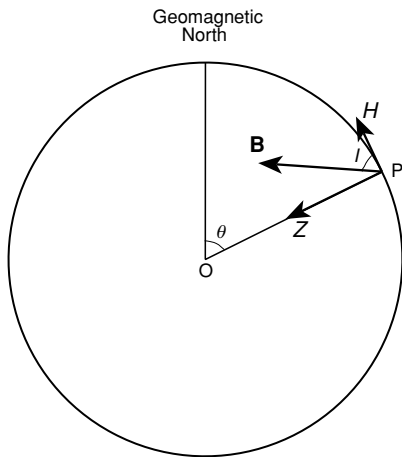
$$B_0 = \frac{\mu_0 m}{4\pi R^3} \quad (3.11)$$

where R is the radius of the Earth, then Eqs. (3.4) and (3.5) give the components of the magnetic field at the Earth's surface:

$$B_r(R, \theta, \phi) = -2B_0 \cos \theta \quad (3.12)$$

$$B_\theta(R, \theta, \phi) = -B_0 \sin \theta \quad (3.13)$$

Figure 3.5. A cross section through the Earth, illustrating the components of the dipole field at a location P on the surface. O is the centre of the Earth, θ the colatitude of P, Z and H are the vertical and horizontal components of \mathbf{B} and I is the angle of inclination.



It follows immediately that, at any point on the Earth's surface, the expression $B_r^2 + 4B_\theta^2$ has the constant value $4B_0^2$. B_0 is most simply visualized in practice as being the equatorial field of the best-fitting dipole field (see Eq. (3.9)). The strength of the field at the poles is about 6×10^{-5} teslas (T) or 6×10^4 nanoteslas (nT) ($1 \text{ weber m}^{-2} = 1 \text{ T}$), and at the equator it is about 3×10^{-5} T (Fig. 3.1(a)).

In geomagnetic work, the inward radial component of the Earth's field is usually called Z (it is the downward vertical at the Earth's surface) and is positive. The horizontal magnitude (always positive) is called H.

Thus, for a dipole,

$$Z(R, \theta, \phi) = -B_r(R, \theta, \phi) \quad (3.14)$$

$$H(R, \theta, \phi) = |B_\theta(R, \theta, \phi)| \quad (3.15)$$

At the surface of the Earth the angle between the magnetic field and the horizontal is called the *inclination* I (Fig. 3.5):

$$\tan I = \frac{Z}{H} \quad (3.16)$$

Substituting for B_r and B_θ from Eqs. (3.12) and (3.13) gives

$$\begin{aligned} \tan I &= \frac{2 \cos \theta}{\sin \theta} \\ &= 2 \cot \theta \\ &= 2 \tan \lambda \end{aligned} \quad (3.17)$$

where λ is the magnetic latitude ($\lambda = 90^\circ - \theta$). Equation (3.17) makes it a simple matter to calculate the magnetic latitude, given the angle of inclination, and vice versa. Mariners use the angle of inclination for navigational purposes.

The angle of *declination* is the azimuth of the horizontal component of the magnetic field. It is measured in degrees east or west of north. Mariners call it the variation or magnetic variation of the compass.⁴ Figure 3.3(b) illustrates

⁴ The magnetic compass was a Chinese invention. Declination was described by Shen Kua in 1088.

how the declination has varied over the last four centuries. In the case of a dipole field aligned along the Earth's rotation axis, the declination would always be zero. Obtaining a very detailed image of the historical magnetic field will not be possible since the measurements were recorded in ship's logs and are therefore necessarily confined to the main shipping and exploration routes.

3.1.3 Magnetization of rocks

Rocks can become permanently magnetized by the Earth's magnetic field. This fact has enabled geophysicists to track past movements of the plates.

As any volcanic rock cools, it passes through a series of critical temperatures at which the various grains of iron minerals acquire spontaneous magnetization. These critical temperatures, called the *Curie points* or Curie temperatures, are different for each mineral (e.g., approximately 580 °C for magnetite (Fe_3O_4) and 680 °C for haematite (Fe_2O_3)). Once the temperature of the rock is lower than the *blocking temperature*, (which for most minerals is tens of degrees less than the Curie point) the magnetized grains cannot be reoriented. This means that the grains have their magnetic moments aligned with the direction the Earth's magnetic field had at the time of cooling. Both of these temperatures are much lower than the temperatures at which lavas crystallize (typically 800–1100 °C), which means that magnetization becomes permanent some time *after* lavas solidify. How long afterwards depends on the physical size and other properties of the intrusion or flow and the rate of cooling, which depends in turn on its environment (see Section 7.8). This type of permanent residual magnetization is called *thermoremanent magnetization* (TRM) and is considerably larger in magnitude than the magnetism induced in the basalt by the Earth's present field.

Sedimentary rocks can also acquire remanent magnetization even though they have never been as hot as 500 °C, but this remanent magnetization of sediments is generally very much less than that of igneous rocks. Sedimentary rocks can acquire magnetization in two ways: *depositional* or *detrital remanent magnetization* (DRM) and *chemical remanent magnetization* (CRM). Detrital remanent magnetization can be acquired, as indicated by its name, during the deposition of sedimentary rocks. If the sediments are deposited in still water, any previously magnetized small grains will align themselves with their magnetic moments parallel to the Earth's magnetic field as they fall. Large grains are unaffected. Chemical remanent magnetization is acquired *in situ* after deposition during the chemical growth of iron oxide grains, as in a sandstone. When the grains reach some critical size, they become magnetized in the direction of the Earth's field at that time. Chemical remanent magnetization is thus a secondary remanent magnetization whereas TRM and DRM are both primary remanent magnetizations dating from the time of formation of the rocks.

The degree to which a rock body can be magnetized by an external magnetic field is determined by the *magnetic susceptibility* of the rock. *Induced*

magnetization is the magnetization of the rock \mathbf{M} which is induced when the rock is put into the Earth's magnetic field \mathbf{B} ; it is given by

$$\mu_0 \mathbf{M}(\mathbf{r}) = \chi \mathbf{B}(\mathbf{r}) \quad (3.18)$$

where χ is the magnetic susceptibility (a dimensionless physical property of the rock). Values of χ for basalts vary from about 10^{-4} to 10^{-1} , so the induced magnetization gives rise to a field that is very much weaker than the Earth's field. Thermoremanent magnetization is generally many times stronger than this induced magnetization. For any rock sample, the ratio of its remanent magnetization to the magnetization induced by the Earth's present field is called the *Königsberger ratio* Q . Measured values of Q for oceanic basalts are in the range 1–160. Thus, an effective susceptibility for TRM of basalt of about 10^{-3} – 10^{-1} appears to be reasonable. This permanent TRM therefore produces a local field of perhaps 1% of the Earth's magnetic field. Effective susceptibilities for sedimentary rocks (DRM and CRM) are about two orders of magnitude less than those for basalt (TRM).

The relationship between the angle of inclination and the magnetic latitude (Eq. (3.17)) means that a measurement of the angle of inclination of the remanent magnetization of a suitable lava or sediment laid down on a continent immediately gives the magnetic palaeolatitude for the particular piece of continent. If the continent has not moved with respect to the pole since the rock cooled, then the magnetic latitude determined from the magnetization of the rock is the same as its present latitude. However, if the continent has moved or if the rock has been tilted, the magnetic latitude determined from the magnetization of the rock can be different from its present latitude. Thus, the angle of inclination provides a powerful method of determining the past latitudes (*palaeolatitudes*) of the continents. Unfortunately, it is not possible to use palaeomagnetic data to make a determination of palaeolongitude.

If the angles of declination and of inclination of our rock sample are measured, the position of the palaeomagnetic pole can be calculated. To do this, it is necessary to use spherical geometry, as in the calculations of Chapter 2. Figure 2.11 shows the appropriate spherical triangle if we assume N to be the present north pole, P the palaeomagnetic north pole and X the location of the rock sample. The cosine formula for a spherical triangle (e.g., Eq. (2.9)) gives the geographic latitude of the palaeomagnetic pole P, λ_p , as

$$\cos(90 - \lambda_p) = \cos(90 - \lambda_x) \cos(90 - \lambda) + \sin(90 - \lambda_x) \sin(90 - \lambda) \cos D \quad (3.19)$$

where λ_x is the geographic latitude of the sample location, D the measured remanent declination and λ the palaeolatitude (given by Eq. (3.17)). Simplifying Eq. (3.19) gives

$$\sin \lambda_p = \sin \lambda_x \sin \lambda + \cos \lambda_x \cos \lambda \cos D \quad (3.20)$$

Example: calculation of palaeomagnetic latitude

Magnetic measurements have been made on a basalt flow at present at 47°N, 20°E.

The angle of inclination of the remanent magnetization of this basalt is 30°.

Calculate the magnetic latitude of this site at the time the basalt was magnetized.

The magnetic latitude λ is calculated by using Eq. (3.17):

$$\tan I = 2 \tan \lambda$$

I is given as 30°, so

$$\begin{aligned}\lambda &= \tan^{-1} \left(\frac{\tan 30^\circ}{2} \right) \\ &= \tan^{-1}(0.2887) \\ &= 16.1^\circ\end{aligned}$$

Therefore, at the time the sample was magnetized, it was at a magnetic latitude of 16°N, which indicates that between then and now the site has moved 31° northwards to its present position at 47°N.

After λ_p has been calculated, the sine formula for a spherical triangle (e.g., Eq. (2.10)) can be used to give the difference between the longitudes of the palaeomagnetic pole and the sample location, $\phi_p - \phi_x$:

$$\begin{aligned}\sin(\phi_p - \phi_x) &= \frac{\sin(90 - \lambda) \sin D}{\sin(90 - \lambda_p)} \\ &= \frac{\cos \lambda \sin D}{\cos \lambda_p} \quad \sin \lambda \geq \sin \lambda_p \sin \lambda_x \\ \sin(180 + \phi_p - \phi_x) &= \frac{\cos \lambda \sin D}{\cos \lambda_p} \quad \sin \lambda < \sin \lambda_p \sin \lambda_x \quad (3.21)\end{aligned}$$

Therefore, by using Eqs. (3.17) and (3.19)–(3.21), we can calculate past magnetic-pole positions.

If palaeomagnetic pole positions can be obtained from rocks of different ages on the same continent, these poles can be plotted on a map. Such a plot is called a *polar-wander path* (a name that is a ‘fossil’ of the older notion that it was the poles, not the continents, that drifted) and shows how the magnetic pole moved relative to that continent. If such polar-wander paths from two continents coincide, then the two continents cannot have moved relative to each other during the times shown. However, if the paths differ, there must have been relative motion of the continents. Figure 3.6 shows polar-wander paths for Europe and North America for the last 550 Ma. Although these two paths have almost the same shape, they are certainly not coincident. When the opening of the Atlantic Ocean is taken into account, however, the two paths can be rotated on top of each other, and they then do approximately coincide.

Example: calculation of latitude and longitude of the palaeomagnetic pole

If the angle of declination for the basalt flow of the previous example is 80° , calculate the latitude and longitude of the palaeomagnetic pole.

The latitude of the palaeomagnetic pole is calculated by using Eq. (3.20) with $\lambda = 16^\circ$ and $D = 80^\circ$:

$$\sin \lambda_p = \sin 47 \sin 16 + \cos 47 \cos 16 \cos 80$$

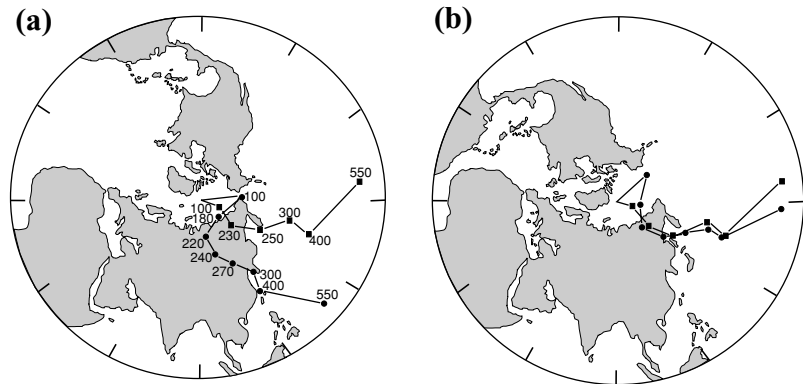
Thus, $\lambda_p = 18^\circ$.

The longitude of the palaeomagnetic pole can now be calculated from Eq. (3.21) after checking whether $\sin \lambda \geq \sin \lambda_p \sin \lambda_x$ or not:

$$\sin(\phi_p - \phi_x) = \frac{\cos 16 \sin 80}{\cos 18}$$

Thus, $\phi_p - \phi_x = 84^\circ$, and so $\phi_p = 104^\circ$. The position of the palaeomagnetic pole is therefore $18^\circ\text{N}, 104^\circ\text{E}$.

Figure 3.6. (a) Polar-wander curves for North America (circles) and Europe (squares). (b) Polar-wander curves for North America and Europe when allowance has been made for the opening of the Atlantic Ocean. The two curves are now almost coincident. (After McElhinny (1973).)



3.2 Dating the oceanic plates

3.2.1 Magnetic stripes

To use measurements of the magnetic field to gain information about the magnetization of the crust, it is first necessary to subtract the regional value of the geomagnetic field (e.g., IGRF 1995). What remains is the magnetic anomaly. Over the oceans, magnetic-field measurements are made by towing a magnetometer behind a ship. A magnetometer can be routinely towed while a research ship is on passage or doing other survey work that does not involve slow, tight manoeuvring. These marine instruments measure the magnitude B , but not the

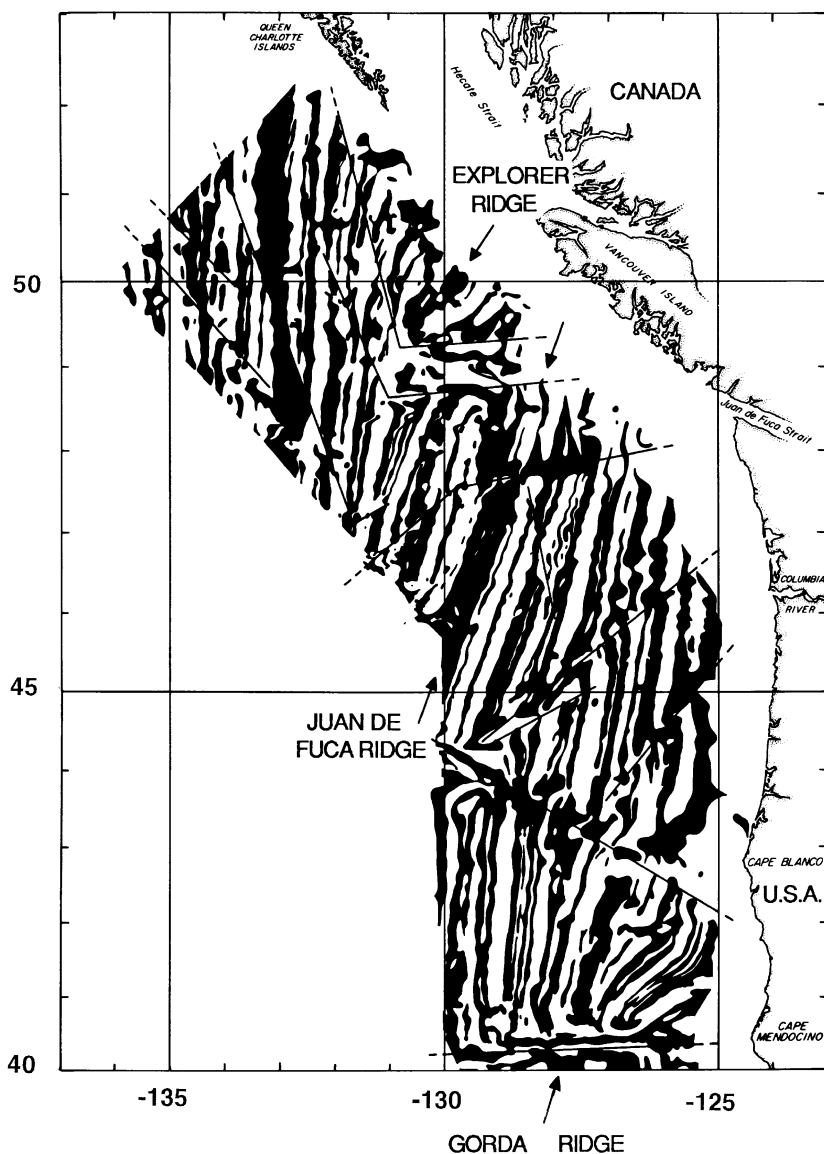


Figure 3.7. Anomalies of the total magnetic field southwest of Vancouver Island in the northeast Pacific Ocean. Positive anomalies are shown in black and negative anomalies in white. Arrows indicate the axes of the three mid-ocean ridges; straight lines indicate the main faults which offset the anomaly pattern. This was the first large-scale map to show the details of the magnetic anomalies over an active mid-ocean ridge. As such it was a vital piece of evidence in the development of the theories of seafloor spreading and then plate tectonics. Compare this with a more recent magnetic-anomaly map for the same area shown in Fig. 3.22. (After Raff and Mason (1961).)

direction, of the total field **B**. (Magnetometers that can measure both magnitude and direction are widely used on land as prospecting tools.) Marine magnetic anomalies are therefore anomalies in the magnitude (or total intensity) of the magnetic field.

The first detailed map of magnetic anomalies off the west coast of North America, published in 1961, showed what was then a surprising feature: alternate stripes of anomalously high and low values of the magnetic field stretching over the entire region (Fig. 3.7). All subsequent magnetic-anomaly maps show that these stripes are typical of oceanic regions. The stripes run parallel to and are

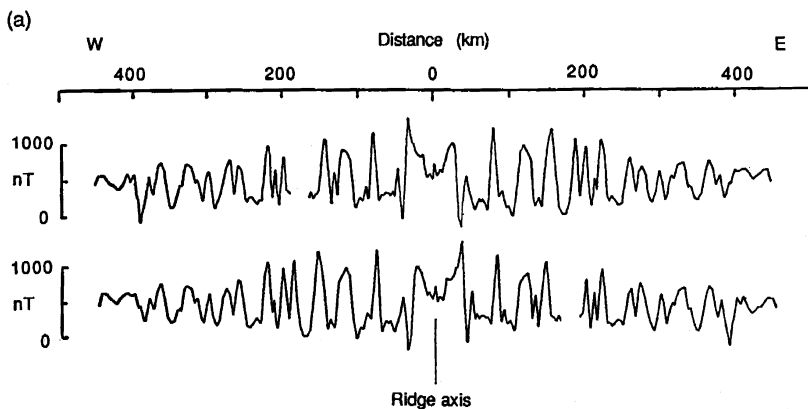


Figure 3.8. (a) A magnetic-anomaly profile across the Pacific–Antarctic Ridge plotted above its end-to-end reverse (mirror image) demonstrates the commonly observed symmetry of magnetic anomalies about the ridge axis. The half-spreading rate as determined from this profile is 4.5 cm yr^{-1} . Magnetic anomalies are generally about $\pm 500 \text{ nT}$ in amplitude, about 1% of the Earth's magnetic field. (After Pitman and Heirtzler (1966).)

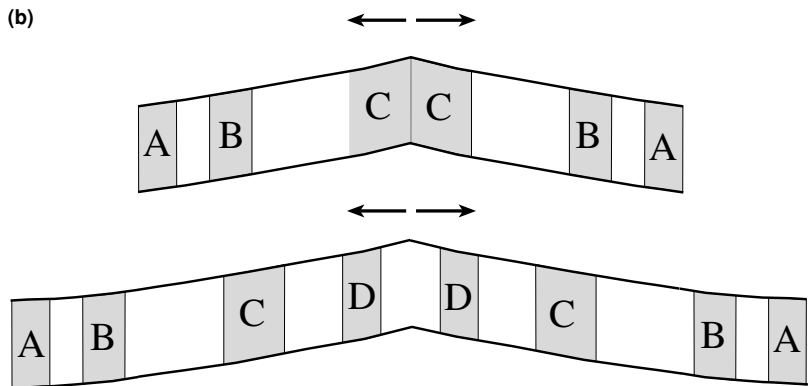


Figure 3.8. (b) A cross section through an idealized ridge illustrates the block model of normally (black) and reversely (white) magnetized material. In the upper drawing, the Earth's magnetic field is positive (normal) and has been for some time; thus, the positively magnetized blocks C have formed. Positively magnetized blocks B and A were formed during earlier times when the Earth's magnetic field also had normal polarity. The lower drawing shows the same ridge at a later time; another positive block D has formed and the magnetic field is in a period of reverse polarity.

generally symmetrical about the axes of the mid-ocean ridges. They are offset by fracture zones, and are a few tens of kilometres in width and typically $\pm 500 \text{ nT}$ in magnitude (Fig. 3.8(a)). This means that magnetic-anomaly maps are very useful in delineation of ridge axes and fracture zones.

The origin of these magnetic stripes was first correctly understood in 1963 by F. J. Vine and D. H. Matthews and independently by L. W. Morley. They realized

that the idea of seafloor spreading, which had then newly been proposed by H. H. Hess, coupled with the then recently discovered evidence that intermittent reversals of the Earth's magnetic field have taken place, provide the answer. The oceanic crust, which is formed along the axes of the mid-ocean ridges as mafic material wells up, acts as a double-headed magnetic tape recorder that preserves the past reversals of the magnetic field on each plate (Fig. 3.8(b)). The width of magnetic stripe is determined by the speed at which 'the tape' is moving (the half-spreading rate) and the length of time between the magnetic reversals. Thus, while the Earth's magnetic field is in its normal polarity, a block of oceanic crust is formed with a strong component of permanent magnetization aligned with the normal field. When the Earth's field is reversed, new oceanic crust will have a strong component of permanent magnetization aligned with the reversed field. In this way a magnetically normal- and reversed-striped oceanic crust is formed, with the stripes parallel to the ridge axis. To 'decode' a magnetic-anomaly pattern, however, it is necessary to know either when the Earth's field reversed, or the half-spreading rate of the ridge.

Example: variability of marine magnetic anomalies

Decoding magnetic anomalies is not as simple in practice as it sounds, partly because the magnetization of the oceanic crust does not conform to a perfect block model. The lava flows that make up the magnetized layer are not produced continuously along the ridge axis. Rather, they are extruded randomly both in time and in space within an *emplacement zone* that is centred on the ridge axis. The effect of this is shown in Fig. 3.9. The simple block model (Fig. 3.8) gives way to a much more complex structure as the width of the emplacement zone is increased. The variability in magnetic anomalies increases accordingly. An emplacement zone 10 km across, which seems to be appropriate for the Mid-Atlantic Ridge, explains the variability of Atlantic magnetic anomalies. Pacific magnetic anomalies are much less variable, partly because the emplacement zone seems to be narrower but mainly because the much faster spreading rate means that the polarity reversals are much more widely spaced.

Nevertheless, the block model for the magnetization of oceanic crust is widely used. All the anomalies shown in the rest of this chapter have been calculated for block models.

By 1966, researchers had established a *reversal timescale* extending back some 4 Ma by using potassium–argon isotopic dating (see Section 6.7) to fit a timescale to the magnetic-reversal sequence that had been measured in continental lava piles and on oceanic islands. This timescale of reversal was then used to interpret oceanic anomalies by calculating theoretical magnetic anomalies for assumed spreading rates and latitudes. Figure 3.10 shows the theoretical

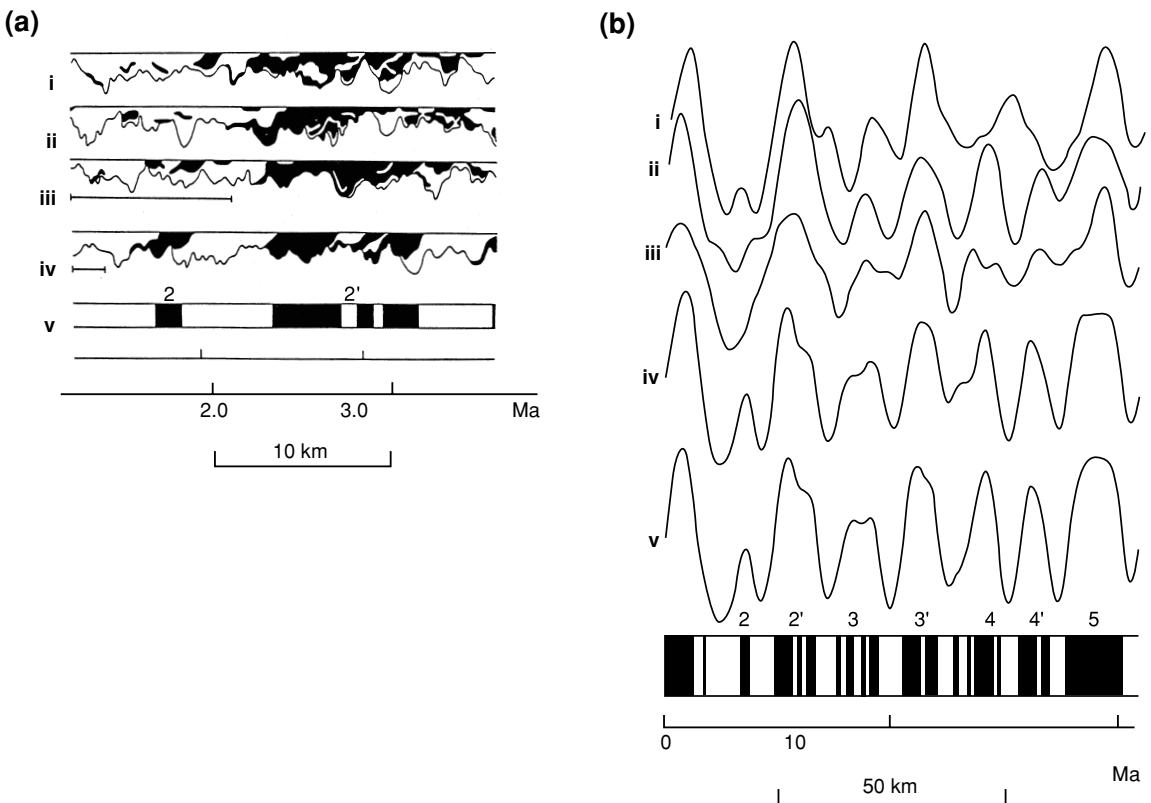


Figure 3.9. (a) A cross section through the upper part of the oceanic crust, showing the magnetized layer generated by extrusion of lava randomly in both time and space within an emplacement zone centred on the ridge axis. The half-spreading rate is 1 cm yr^{-1} . Black, normally magnetized rock; white, reversely magnetized rock. (b) Theoretical magnetic anomalies generated by this random-extrusion model. In both (a) and (b), (i), (ii) and (iii) are for an emplacement zone 10 km across, (iv) is for an emplacement zone 2 km across and (v) is for the block model in which the emplacement zone has zero width. (From Schouten and Denham (1979).)

anomalies calculated for the Juan de Fuca Ridge and the East Pacific Rise using this 1966 reversal timescale. These theoretical anomalies match the actual anomalies very well and were used to confirm the *Vine–Matthews hypothesis*. Figure 3.11 shows a more recent (and therefore more detailed) determination of the reversal sequence for the last 4 Ma.

A geomagnetic timescale extending back 80 Ma was first established in 1968 by assuming that the spreading rate in the South Atlantic had remained constant from 80 Ma until now. The observed anomaly pattern was matched with theoretical profiles computed for a sequence of normal and reversed magnetized blocks symmetrical about the Mid-Atlantic Ridge axis (Fig. 3.12). The timescale derived

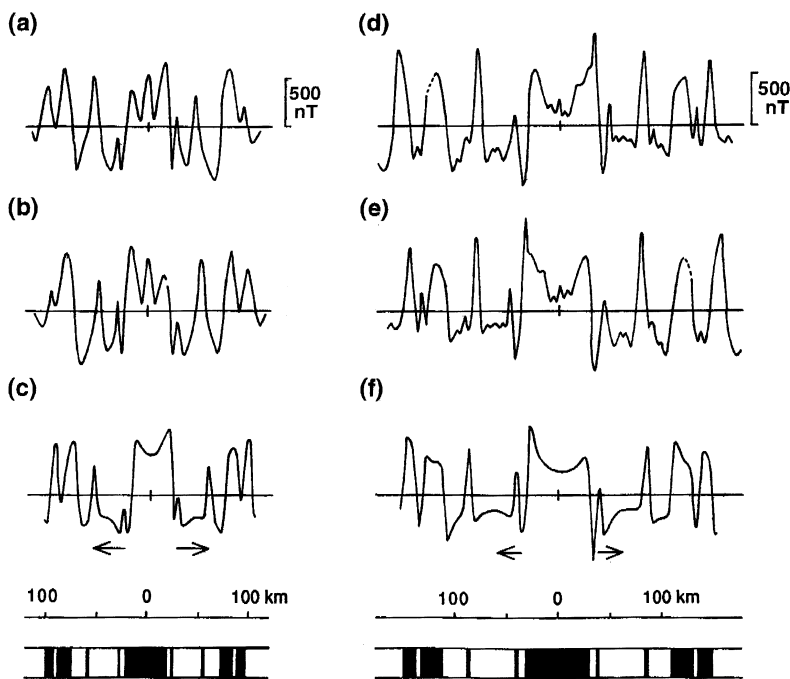
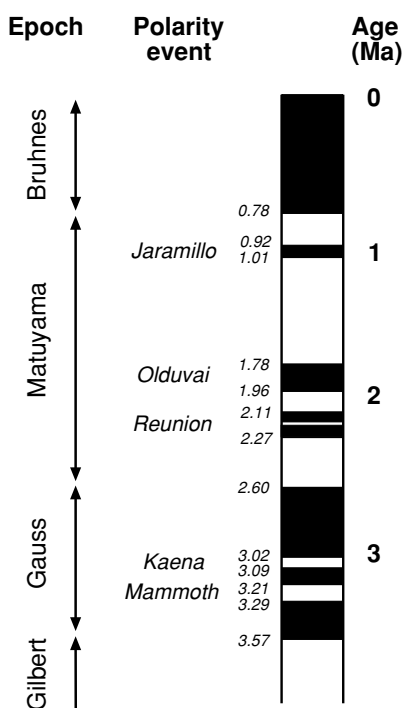


Figure 3.10. (a) The magnetic-anomaly profile over the Juan de Fuca Ridge at 46°N, southwest of Vancouver Island, Canada. (b) The profile in (a) is reversed; note the symmetry. (c) A model magnetic-anomaly profile calculated for this ridge assuming a half-spreading rate of 2.9 cm yr^{-1} and the magnetic-reversal sequence shown below. On the magnetic-reversal timescale, black blocks represent periods of normal polarity and white blocks periods of reverse polarity. (d) The magnetic-anomaly profile over the East Pacific Rise at 51°S. (e) The profile in (d) is reversed; note the symmetry. (f) A model magnetic-anomaly profile calculated for this ridge assuming a half-spreading rate of 4.4 cm yr^{-1} and the magnetic-reversal sequence shown below. The magnetic-reversal timescale is the same as that for the Juan de Fuca Ridge (see (c)), but with a different horizontal scale because of the faster spreading rate. (After Vine (1966).)

from this model and the whole seafloor-spreading hypothesis were spectacularly confirmed by drilling the ocean bottom as part of the Deep Sea Drilling Project (DSDP), an international enterprise that began in 1968 (see Section 9.2.1). During Leg 3 of the DSDP a series of holes was drilled into the basalt at the top of the oceanic crust right across the Atlantic at 30°S (Fig. 3.13). It was not possible to use radiometric methods to date the lavas sampled from the top of the crust because they were too altered; instead, the basal sediments were dated using fossils. The ages are therefore slightly younger than the lava ages would have been. Figure 3.13(b) shows these sediment ages plotted against the distances of their sites from the ridge axis. The straight line confirmed that spreading in the

Figure 3.11. Details of the recent reversals of the Earth's magnetic field as determined from detailed radiometric dating of continental and oceanic-island lavas and palaeomagnetism of marine sediments. The *epochs*, time intervals during which the Earth's magnetic field was either predominantly normal or predominantly reversed in polarity, have been named after prominent scientists in the study of the Earth's magnetic field. (William Gilbert was a sixteenth-century English physician, Carl Friedrich Gauss was a nineteenth-century German mathematician, Bernard Brunhes (1906) was the first person to propose that the Earth's magnetic field was reversed at the time lavas were formed and Motonori Matuyama (1929) was the first person to attempt to date these reversals.) The *polarity events* (*subchrons*), short fluctuations in the magnetic polarity, are named after the geographic location where they were first recognized (e.g., Olduvai Gorge, Tanzania, the site of the early hominid discoveries of Leakey; Mammoth, California, U.S.A.; and Jaramillo Creek, New Mexico, U.S.A.). (Based on McDougall *et al.* (1992) and Spell and McDougall (1992).)



South Atlantic had been continuous and had been occurring at a fairly steady rate for the last 80 Ma, and that the geomagnetic timescale (Fig. 3.12) was reasonably accurate. Since then, considerable effort has been put into ensuring that geological and magnetic timescales are as precise as possible. Figure 3.14 shows a timescale from the middle Jurassic to the present.

To use a geomagnetic timescale to date the oceanic plates, it is necessary to recognize specific anomalies. Fortunately, the reversal sequence is sufficiently irregular (Fig. 3.14) for this to be possible for the trained eye. The prominent anomalies up to age 83 Ma have been numbered from one to thirty-three. For ages 125–162 Ma they are labelled with the prefix M (M standing for Mesozoic). Particularly prominent is the long Magnetic Quiet Zone in the Cretaceous (83–124 Ma numbered C34), during which no reversals occurred.

Figure 3.12 showed profiles from the Pacific and their corresponding theoretical profiles, as well as the South Atlantic profiles. It is clear that, in contrast to the history of the Atlantic, spreading rates in the Pacific have changed markedly with time. This is also the case in the Indian Ocean. Figure 3.15 is an isochron map of the ocean floor. This shows that the ridges have undergone a number of changes both in rate and in direction of spreading in the past. The oldest parts of the ocean floor are Jurassic. This is an interesting fact in itself and the subject of conjecture about the density and stability of older oceanic lithosphere and causes of initiation of a subduction zone in any particular location.

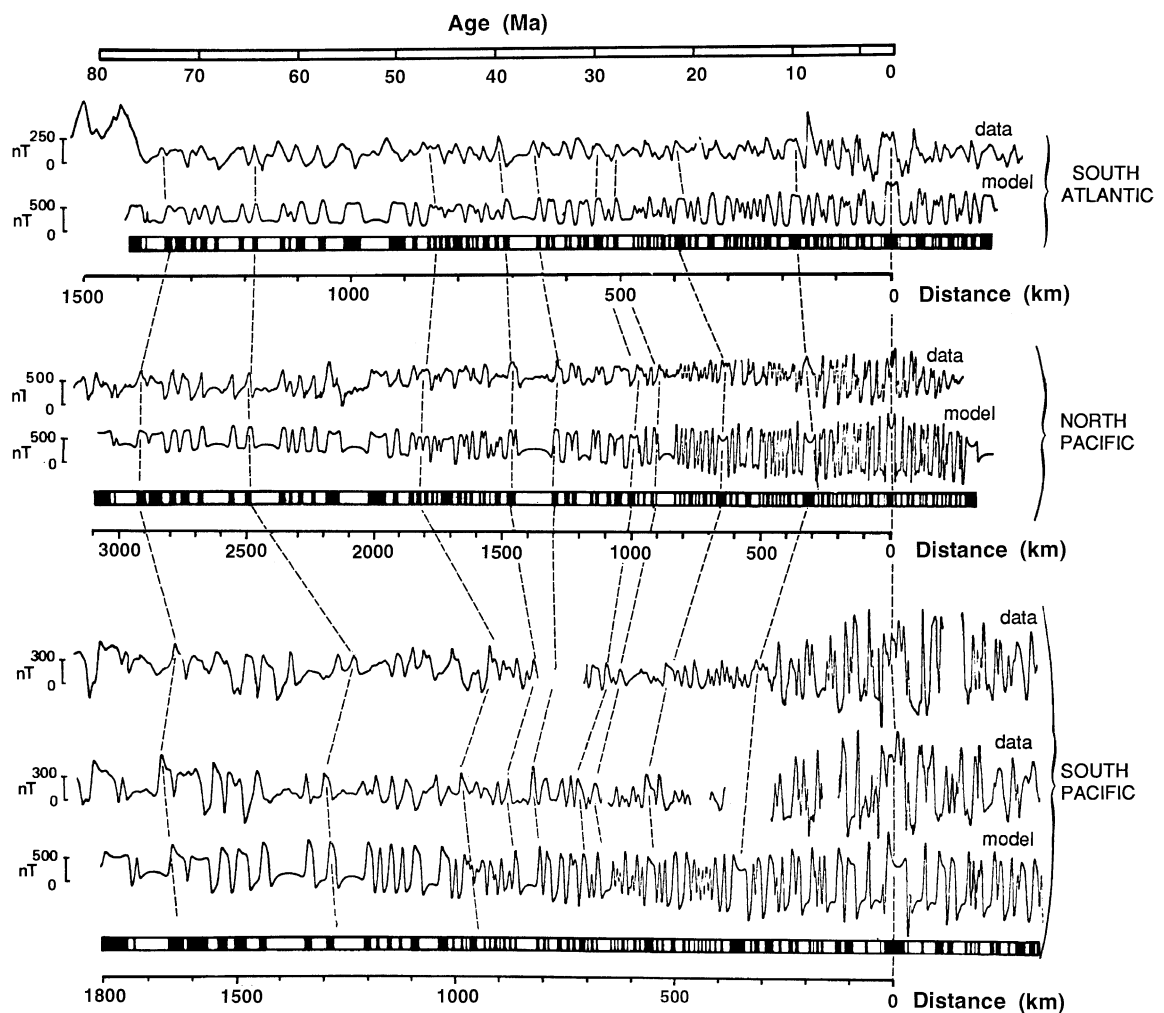


Figure 3.12. The geomagnetic-reversal timescale for the last 80 Ma as proposed in 1968. The magnetic-anomaly profiles with their model profiles and model reversal sequences are shown for the South Atlantic, North Pacific and South Pacific. The South Atlantic timescale was made by assuming that the spreading rate there has been constant for the last 80 Ma. In comparison, spreading in the Pacific has clearly been both faster and more irregular (note the different distance scales for the Pacific data). Dashed lines connect specific magnetic anomalies numbered as in Fig. 3.14. (After Heirtzler *et al.* (1968).)

3.2.2 Calculation of marine geomagnetic anomalies

The marine magnetic-anomaly patterns (e.g., Figs. 3.10 and 3.12) can give immediate values for the relative motion between two plates if specific anomalies can be identified and if the reversal timescale is known. The patterns can also be used to estimate the relative motion between the plate and the Earth's magnetic pole. This

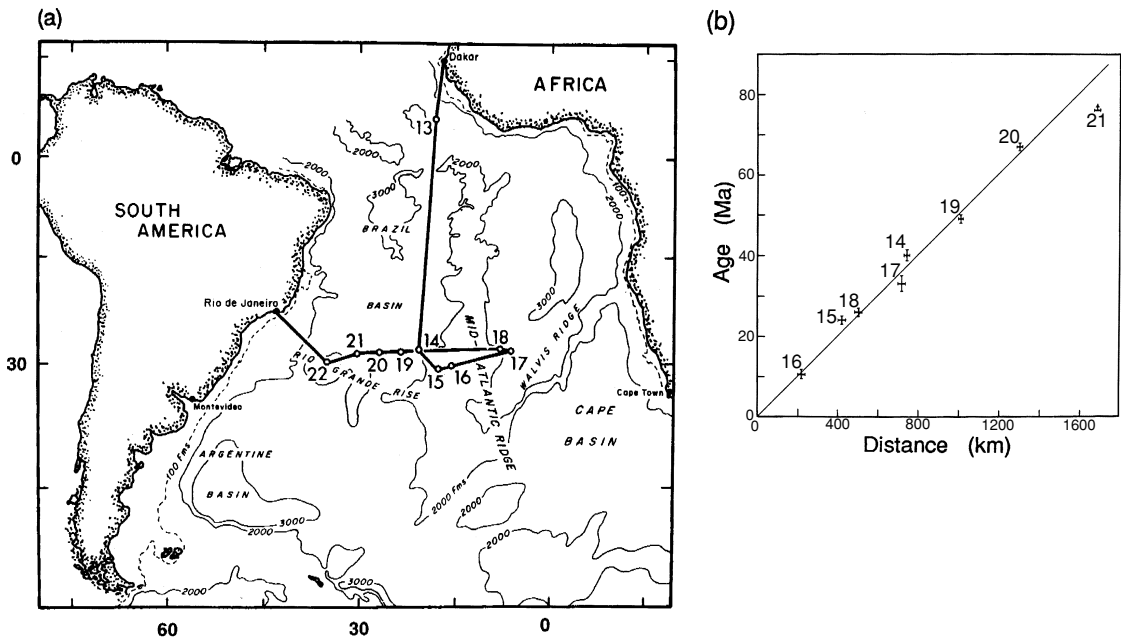


Figure 3.13. (a) Geographic locations of the drilling sites on Leg 3 of the Deep Sea Drilling Project. Site numbers refer to the order in which the holes were drilled. (b) The age of the sediment immediately above the basalt basement versus the distance of the drill site, as shown in (a), from the axis of the Mid-Atlantic Ridge. (From Maxwell *et al.* (1970).)

follows in the same way as that in which the remanent magnetization of continental lavas gives their magnetic latitude (Eq. (3.17)). The magnitude and direction of the remanent magnetization of oceanic crust depend on the latitude at which the crust was formed and are unaffected by later movements and position. This means that, although the magnetic anomaly resulting from this magnetization of the crust is dependent on the present location of that piece of crust, it can be used to determine the original latitude and orientation of the mid-ocean ridge, though not the longitude.

Imagine a mid-ocean ridge spreading symmetrically, producing infinitely long blocks of new crust (Fig. 3.16). The magnetic field measured above any block will include a contribution from the permanent magnetization of the block. Suppose first that, at the time the block was formed, the ridge was at the equator, where the magnetic field is north–south and has no vertical component (Eq. (3.9)), and was spreading east–west. In this case, the permanent magnetization of the block would be along the block, $\mathbf{M} = (0, M_y, 0)$, and so the magnetic field lines cannot leave the block (the block being infinitely long). It is therefore impossible for the magnetic field of this block to affect the magnetic field outside the block. Such a block would not produce an anomaly!

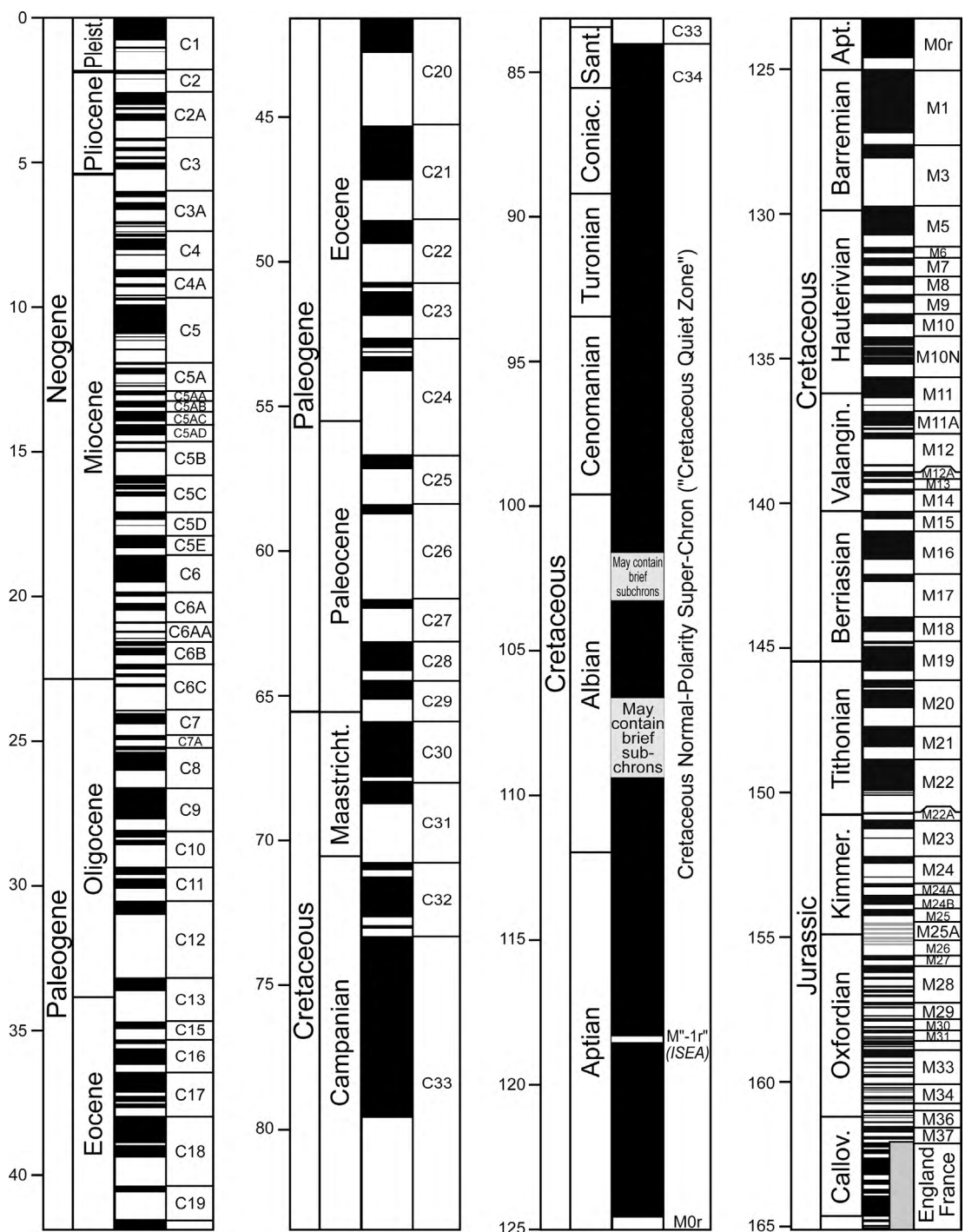


Figure 3.14. The geomagnetic-reversal time scale. Black indicates periods of normal polarity for the Earth's magnetic field; white, reversed-polarity periods. The grey pattern indicates uncertain polarity. The anomaly or chron numbers, C1–C34 and M0–M38, are on the right-hand side of the columns; the age (in Ma) is along the left-hand side. Note that the International scale uses not 'Tertiary' and 'Quaternary' but 'Paleogene' and 'Neogene'. (By Gabi Ogg, after Gradstein *et al.* 2004, *Geologic Time Scale 2004*.)

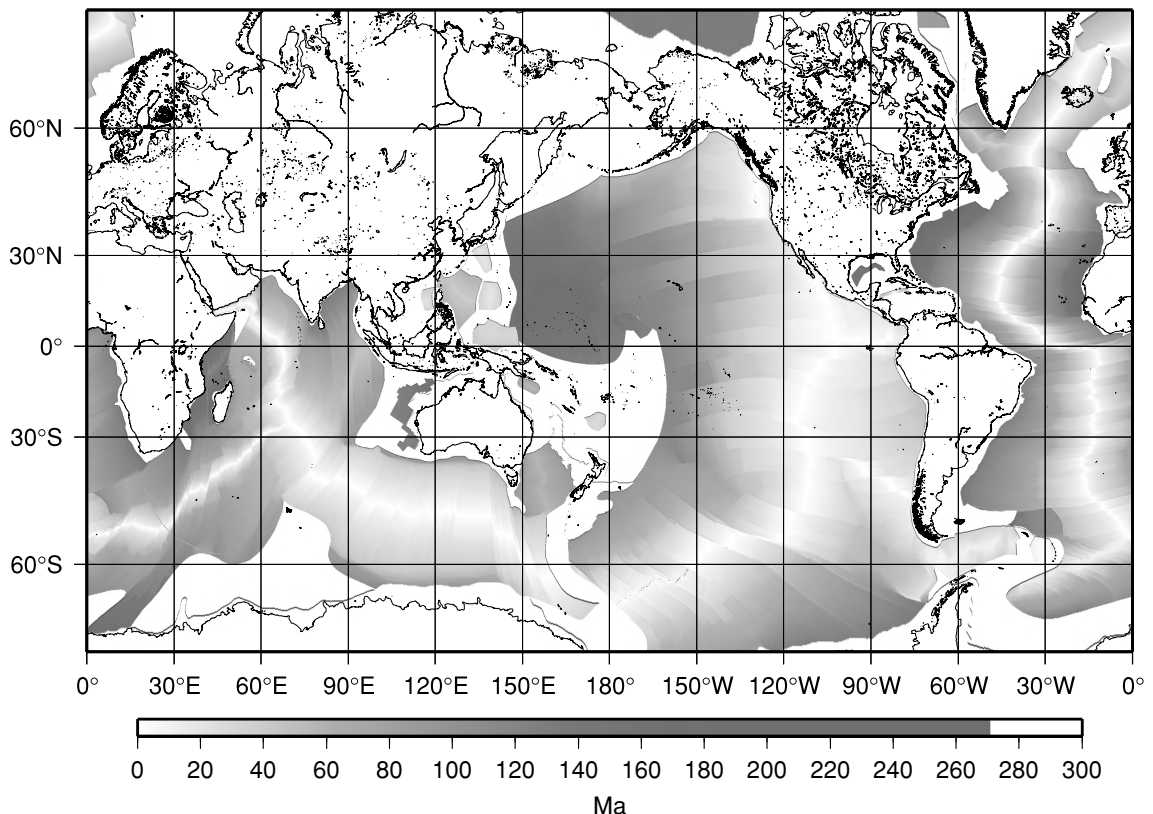


Figure 3.15. The age of the ocean floor determined using magnetic-anomaly data, basement ages from deep-sea drilling, anomaly timescales and rotation poles and angles. For a colour version see Plate 2. (R. D. Müller, personal communication 2004, after Muller *et al.* (2002).)

Now imagine another ridge, still spreading east–west, but not at the equator. Because, in this example (as in the previous one), the ridge is striking north–south, the horizontal remanent magnetization is in the y direction and has no component in the x direction (because $B_\phi = 0$). As before, magnetization in the y direction cannot affect the magnetic field outside the block (the block being infinitely long) and so it is only the vertical component of the remanent magnetization that affects the magnetic field outside the block. The vertical component of the magnetic field as measured today by a ship above the block will be either reduced or increased, depending on whether the magnetic field at the time the block was formed was reversed or normal. The magnetic anomalies produced by a symmetrical pattern of such blocks from an east–west spreading ridge are symmetrical.

For all spreading directions of the ridge that are not east–west, there is a component of the remanent magnetization in the x direction. The effect of this

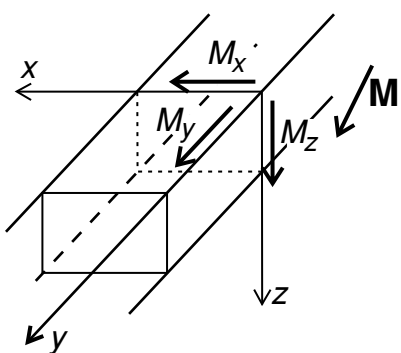


Figure 3.16. An infinitely long block of magnetized oceanic crust. The magnetization of the block \mathbf{M} is resolved into three components (M_x , M_y and M_z). M_y is the horizontal component parallel to the block and so cannot contribute to the magnetic field outside the block. M_z (the vertical component) and M_x (the horizontal component perpendicular to the block) both contribute to the magnetic field outside the block and hence to the resultant magnetic anomaly produced by the block.

component M_x is complicated, but it usually produces an asymmetry in the magnetic anomalies. In the vicinity of the magnetic poles, where the Earth's magnetic field is almost vertical, the effects of the x component of magnetization are almost negligible; however, close to the magnetic equator the effect becomes important.

Calculation of synthetic magnetic anomalies for any general block model (e.g., Fig. 3.8(b)) is performed in the following way.

1. Calculate remanent magnetization in the x and z directions for each block by assuming the orientation and latitude at which blocks were formed.
2. Calculate the field produced by these blocks along a line perpendicular to the blocks and at a constant distance above them (i.e. sea-surface level).
3. Add this field to the Earth's magnetic field (e.g., IGRF 1995) at the block's present-day latitude. This is the field that would be 'measured'.
4. Calculate the difference in magnitude between this 'measured' field and the Earth's field. (For more details, see McKenzie and Sclater (1971).)

To visualize the effect of present-day latitude on the magnetic anomalies produced by a given block structure, consider a model oceanic crust formed by east–west spreading of a mid-ocean ridge at 40°S. Figure 3.17 shows the magnetic anomalies that this magnetized oceanic crust would produce if it later moved north from 40°S. The present-day latitude is clearly an important factor in the shapes of the anomalies; note in particular that, if the plate moves across the equator, positively magnetized blocks give rise to negative anomalies, and vice versa. (This is a result of B_r at today's latitude and M_z having opposite signs.)

Magnetic anomalies are dependent on the orientation of the ridge at which the crust was formed as well as the latitude. The orientation determines the relative values of M_x and M_y . Figure 3.18 shows anomalies that would be observed at 15°N. The magnetized blocks were produced by ridges at 40°S, striking in the three directions shown. The anomalies produced by the ridge striking N45°E and the ridge striking N45°W are identical. This ambiguity in the strike of the ridge

Figure 3.17. Synthetic magnetic-anomaly profiles generated by a ridge at 40° S, spreading east–west with a half-rate of 3 cm yr^{-1} . The magnetized crust subsequently moved northwards to the latitudes shown, leaving the blocks striking north–south. Note that the shapes of the anomalies depend upon the present latitude and that, if the magnetized crust moves across the equator, positively magnetized blocks give rise to negative anomalies. Black denotes periods of normal magnetic field; white denotes periods of reversed field. Numbers are anomaly numbers (see Fig. 3.14). (From McKenzie and Sclater (1971).)

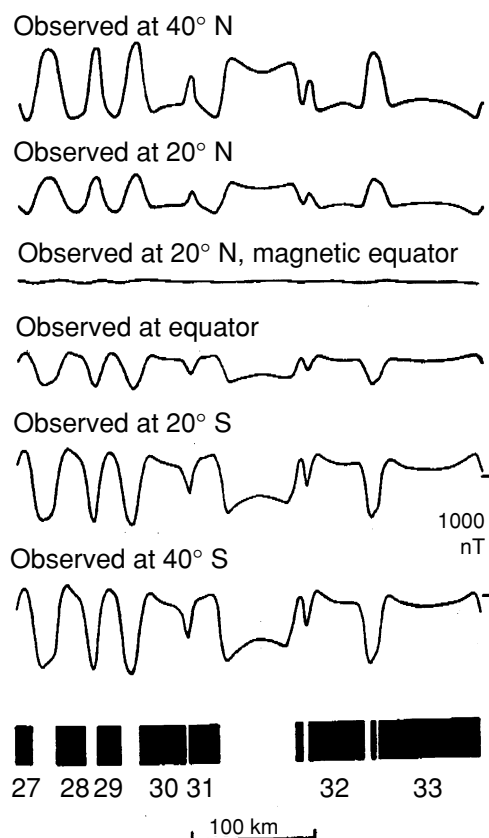
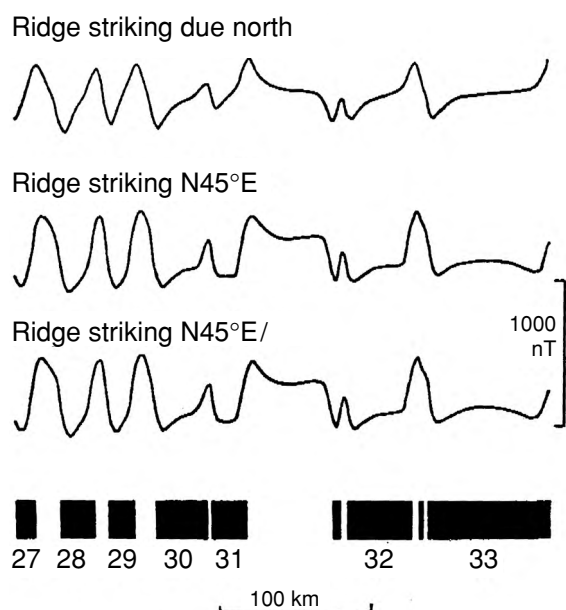


Figure 3.18. Synthetic magnetic-anomaly profiles produced by the magnetized blocks now striking east–west at 15° N. The magnetized oceanic crust was formed at 40° S by mid-ocean ridges spreading at 3 cm yr^{-1} half-rate and striking due north, $N45^{\circ}$ E and $N45^{\circ}$ W. Note that the anomalies for the $N45^{\circ}$ E ridge and the $N45^{\circ}$ W ridge are exactly the same. Numbers are anomaly numbers (see Fig. 3.14). (From McKenzie and Sclater (1971).)



is always there: Anomalies from a ridge striking $-\alpha$ could also have come from a ridge striking $+\alpha$.

The thickness of the magnetized blocks that give rise to the oceanic magnetic anomalies is not well determined. In general, the anomalies depend primarily on the product of the magnetic susceptibility and layer thickness (i.e., 400 m of material with a susceptibility of 0.05 gives rise to almost the same magnetic anomaly as 2 km of material with a susceptibility of 0.01). At one time it was thought that the magnetized layer was only the very top of the oceanic crust (then termed layer 2A, discussed in Section 9.2.1) but this is not now thought necessarily to be the case. The axial magnetization is generally greater than magnetization of old oceanic crust. This high-amplitude axial anomaly/magnetization is probably caused by highly magnetized extrusive basalts. The high magnetization of young basalts of $20\text{--}30 \text{ A m}^{-1}$ decays rapidly within the first few million years. This initial decay is then followed by a slow long-term decay in amplitude with age until magnetization of $3\text{--}6 \text{ A m}^{-1}$ is reached. This later decay may be due to low temperature and hydrothermal oxidation of the magnetic mineral magnetite. Over old oceanic crust the main source of magnetic anomalies may be deeper gabbros, rather than the uppermost crust.

3.3 Reconstruction of past plate motions

3.3.1 Introduction

A magnetic-anomaly profile can be used to construct a magnetized block model of the ocean crust and to estimate the latitude and orientation of the mid-ocean ridge which produced it. When several profiles are available and the magnetic anomalies are plotted on a map, as in Fig. 3.7, such a block model is easily visualized. To determine the past movements of plates, a substantial amount of palaeomagnetic data is required. This data collection began with the development of magnetometers, by Bell Telephone Labs and Gulf Oil, to detect submarines. The instruments were required to measure magnetic fields to about 1 nT (about one part in 50 000), which was ideal for measuring marine magnetic anomalies.

Since the oldest oceanic lithosphere is Jurassic ($\sim 160 \text{ Ma}$ old), magnetic-anomaly data can only be used to trace the past motions of the plates back to that time. Continental magnetic data and other geological data provide evidence for motions of the plates prior to the Jurassic, but the data are necessarily sparser and more difficult to interpret. The remainder of this chapter provides sections on the geological histories of the Pacific, Indian and Atlantic Oceans as established by deciphering magnetic anomalies. The full reconstruction of the geological history of an ocean is possible only if the ocean contains only ridges. For oceans such as the Indian and Pacific, in which subduction has taken place, there has been a loss of information, which prevents a full reconstruction. Deciphering the geological histories of the oceans, especially the early work by McKenzie and Sclater on the Indian Ocean, was one of the triumphs of plate tectonics.

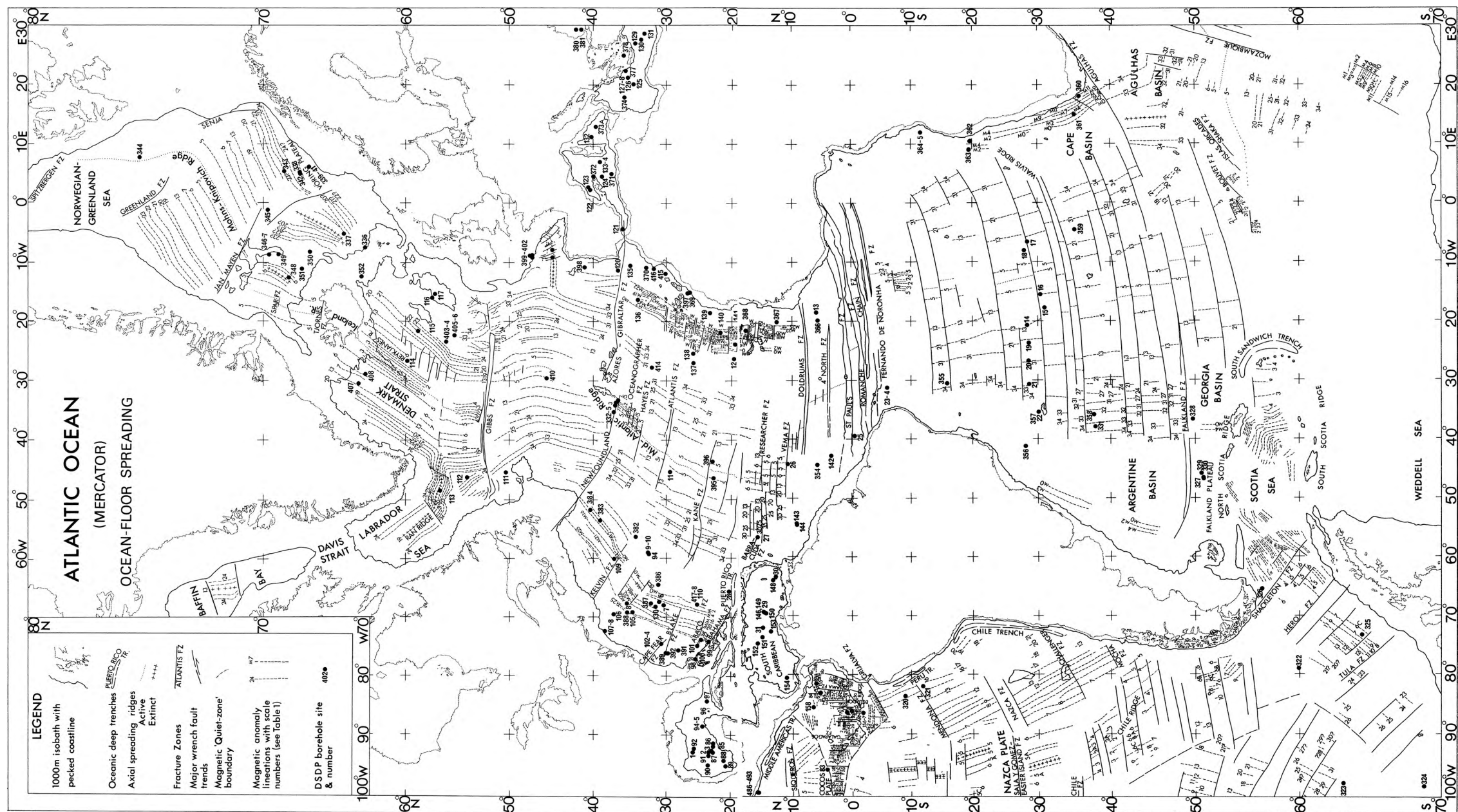


Figure 3.19. Magnetic anomalies, fracture zones and DSDP borehole sites in the Atlantic Ocean. (From Owen (1983).)

3.3.2 The Atlantic Ocean

The magnetic-anomaly map of the Atlantic Ocean is by far the simplest for the three major oceans (Fig. 3.19). The history of continental splitting and seafloor spreading is almost completely preserved because, apart from the short lengths of the Puerto Rico Trench and the South Sandwich Trench, there are no subduction zones. The Mid-Atlantic Ridge is the plate boundary between the Eurasian, African and North and South American plates. Despite the changes in pairs of plates, the poles and instantaneous rotation rates are such that the spreading rate of the Mid-Atlantic Ridge does not vary greatly along its length. The boundary between the North American and the South American plates is best described as a ‘diffuse plate boundary’ between the Mid-Atlantic Ridge and the Caribbean.

The oldest identified anomaly in the South Atlantic is M11, which occurs just off the west coast of South Africa. Thus, Africa and South America must have started separating shortly before this time (135 Ma). The oldest anomaly in the central Atlantic is M25, identified off the east coast of North America and the northwest coast of Africa. Africa and North America therefore started to separate during the mid Jurassic, probably soon after 180 Ma. This motion resulted in considerable faulting and folding in the Mediterranean region because the early stage of rifting between Eurasia and North America did not begin until much later (\sim 120–140 Ma). Rifting then proceeded northwards in stages. The Reykjanes Ridge between Greenland and Eurasia started spreading at about 55 Ma. The northwest–southeast anomalies in the Labrador Sea between Canada and Greenland (anomalies 27–19) and extending northwards into Baffin Bay (anomalies 24–13) indicate that there was also an active ridge there from about 60 Ma until 43 or 35 Ma. Since this time, Greenland has not moved independently and has been part of the North American plate: the spreading that started with anomaly 24 has continued only along the Reykjanes Ridge. North of Iceland the Arctic ridge system includes the Kolbeinsey, Mohns, Knipovitch and Gakkel Ridges (Fig. 2.2).

3.3.3 The Indian Ocean

The magnetic-anomaly map of the Indian Ocean (Fig. 3.20) is considerably more complex than that of the Atlantic Ocean. The three present-day mid-ocean ridges – the Central Indian Ridge, Southwest Indian Ridge and Southeast Indian Ridge – intersect at the Indian Ocean (or Rodriguez) Triple Junction (Fig. 2.2), an RRR triple junction. The Southeast Indian Ridge is spreading fairly fast (3 cm yr^{-1} half-rate) and has smooth topography, whereas the Southwest Indian Ridge is spreading very slowly (0.6–0.8 cm yr^{-1} half-rate) and has rough topography and many long fracture zones. The Carlsberg Ridge starts in the Gulf of Aden and trends southeast. At the equator it is intersected and offset by many transform faults, so the net strike of the plate boundary between Africa and

India becomes almost north–south. This part of the plate boundary is called the Central Indian Ridge. The Southwest Indian Ridge, which extends from the Bouvet Triple Junction in the South Atlantic to the Indian Ocean Triple Junction, is the boundary between the African and Antarctic plates. The position of the present-day rotation pole for Africa relative to Antarctica at about 6°N, 39°W (Table 2.1) means that this ridge is offset by a series of very long transform faults. One of the main fault complexes, the Andrew Bain Fracture Zone, offsets the ridge axis by some 500 km. The half-spreading rate in this region is about 0.8 cm yr⁻¹. The African is subdivided into the Nubian and Somalian plates (Sect. 10.4.2). The triple junction between the Nubian, Somalian and Antarctic plates is located within the Andrew Bain Fracture zone at ~30° E. The other major bathymetric features of the Indian Ocean are the Ninety-East Ridge and the Chagos–Maldives–Laccadive Ridge system. Both of these linear north–south submarine mountain chains are hotspot tracks – of the Kerguelen and Réunion hotspots, respectively.

The oldest magnetic anomalies in the Indian Ocean occur in the Wharton basin (M9–M25), which lies between Australia and the Java Trench, west of Western Australia (M0–M22), between Madagascar and east Africa (M2–M22), in the Somali basin (M13–M21) and north of Antarctica at 20°E (M1–M16). These anomalies indicate that the separation of Africa and Antarctica began by the time of anomaly M21 (150 Ma). At this time, east Antarctica and Madagascar (then joined) moved southwards away from Africa (Fig. 3.21(a)). In so doing, they generated the symmetrical anomalies in the Somali basin, as well as those off the east Antarctic coast and west of Madagascar, which appear to be the northern and southern halves of a symmetrical pattern. At about the time of anomaly M0, seafloor spreading in the Somali basin north of Madagascar stopped and a new ridge was initiated between Madagascar and Antarctica: the proto-Southwest Indian Ridge formed, separating Antarctica from Africa, Madagascar and India. From the time of anomaly 34 (~90 Ma) until the present, spreading along this ridge appears to have been fairly constant, but magnetic-anomaly data from this ridge are very scarce.

The anomalies north of Australia, to the north and east of the Exmouth Plateau, M9–M25, are only the southern half of a symmetrical pattern; the northern part has been subducted by the Java Trench, which is currently active there. The oldest anomaly close to the continental margin north of Australia, M25, gives an estimate of the date of opening of this ocean as 155 Ma. A northeast–southwest pattern of anomalies (M11–M0) is present in the Bay of Bengal and west of Western Australia there is a symmetrical pattern of anomalies M0–M10. This indicates that a ridge was active here by M10 time (134 Ma). This ridge was the plate boundary between the Indian plate and the Australia–Antarctic plate. Australia and Antarctica were still joined at this stage, though continental extension had been taking place since the separation of India (Fig. 3.21(b)).

At about 96 Ma a major change in the plate motions occurred; and the major part of the Indian Ocean has been created since then. At this time (or shortly

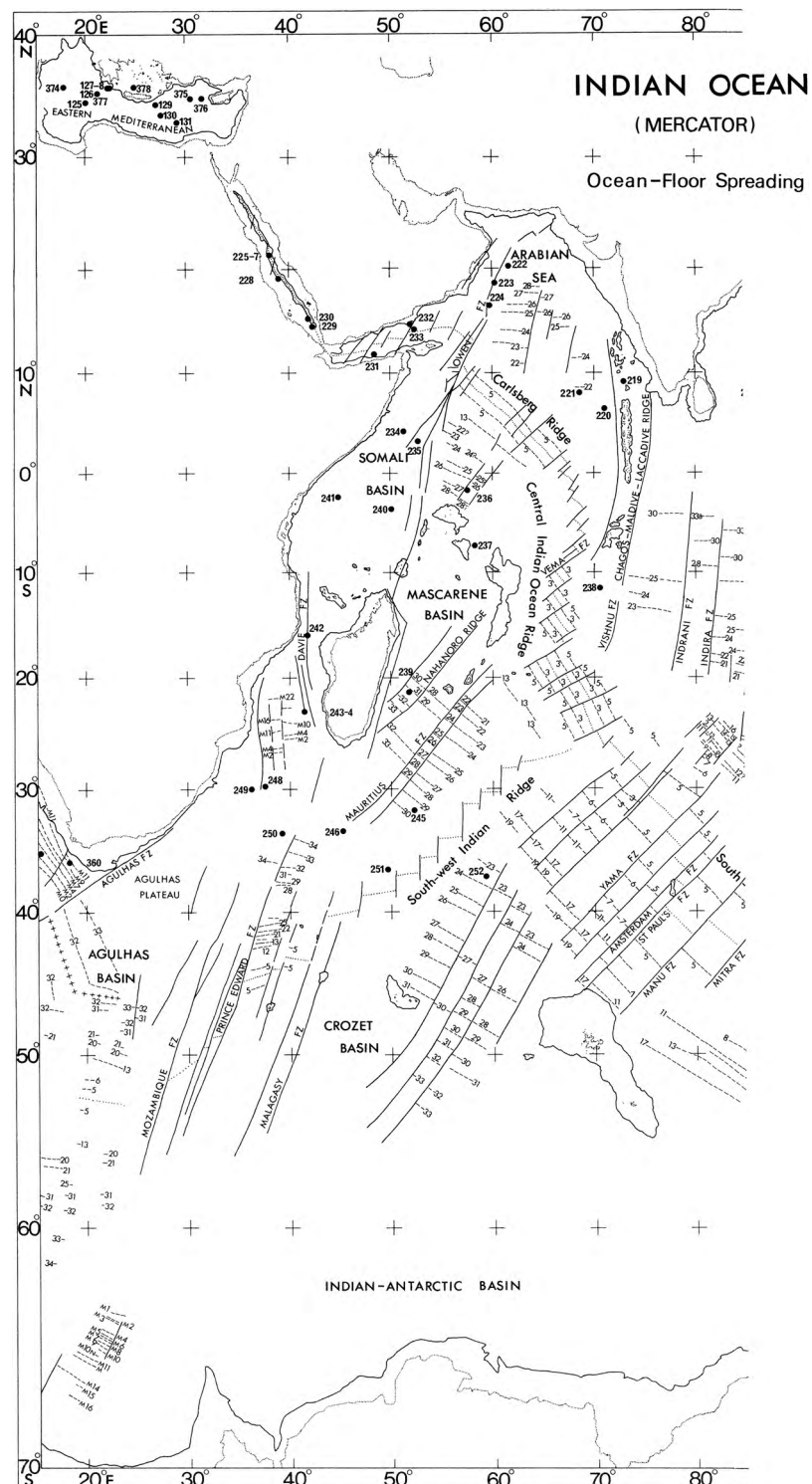
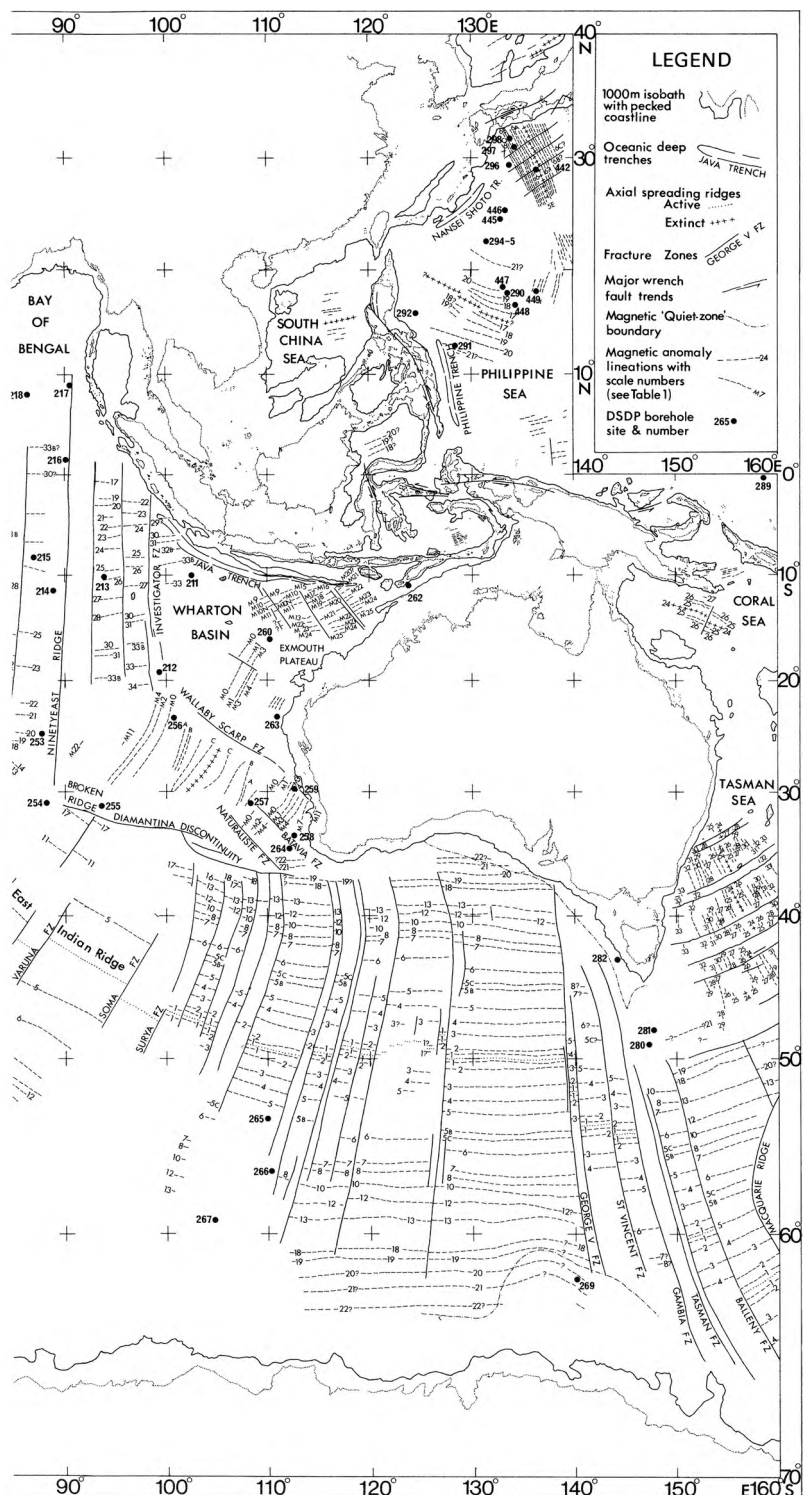


Figure 3.20. Magnetic anomalies, fracture zones and DSDP borehole sites in the Indian Ocean. (From Owen (1983).)



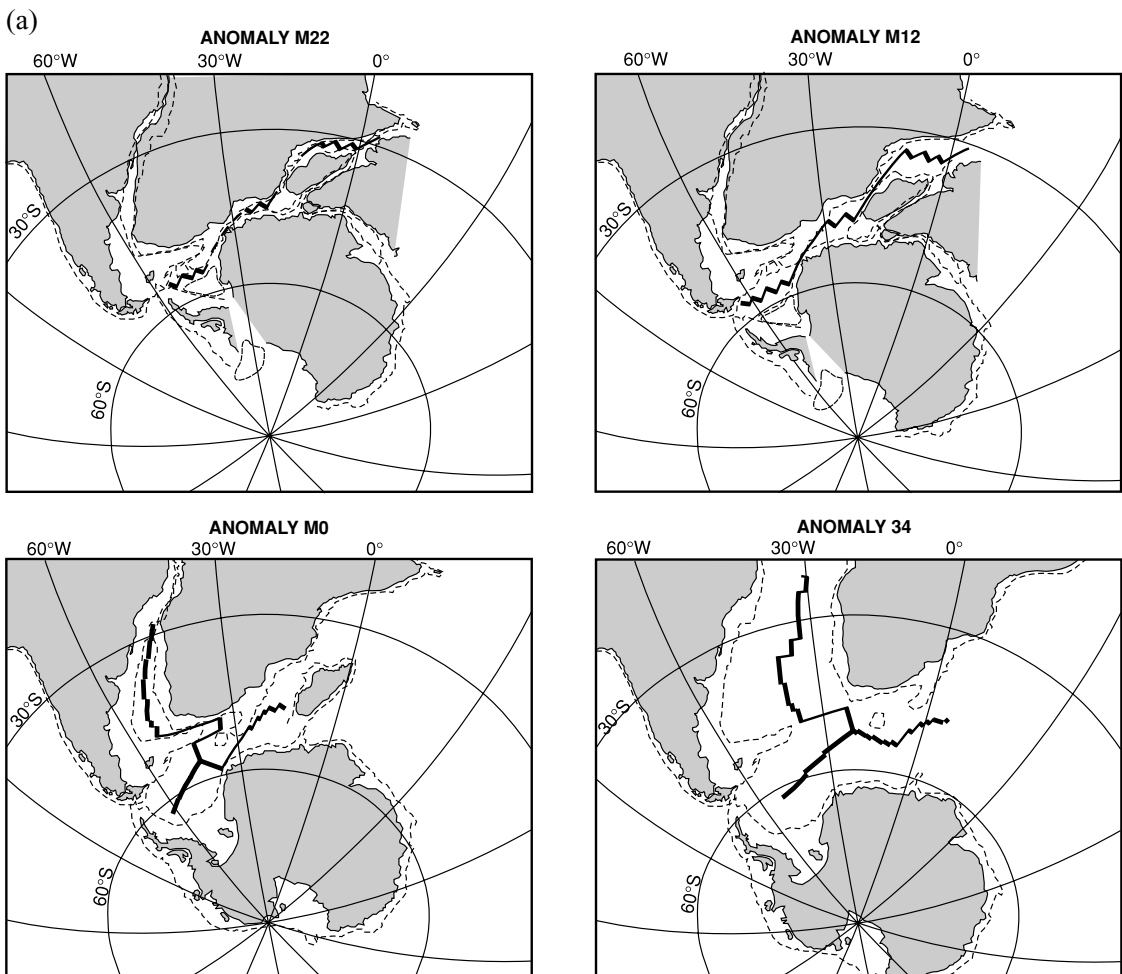


Figure 3.21. (a) Reconstructions of the positions of South America, Africa and Antarctica at the time of anomalies M22, M12, M0 and 34. (From Lawver *et al.* (1985).)

before, as anomaly information is not available for the Magnetic Quiet Zone), the Southeast Indian Ridge started spreading. This began the splitting of Australia from Antarctica. At the same time, India began to move rapidly northwards from Antarctica. The Carlsberg–Central Indian Ridge also started spreading, separating Africa from India. The half-spreading rate of the portion of the Southeast Indian Ridge between Australia and Antarctica was slow (perhaps only 0.5 cm yr^{-1}), whereas the spacing of the same anomalies to the south and east of India indicates half-spreading rates of 10 cm yr^{-1} or more for the ridge between India and Antarctica (Fig. 3.21(b)). Figure 3.21(c) illustrates the relationship between the Réunion hotspot and the Deccan Traps, a very major flood-basalt

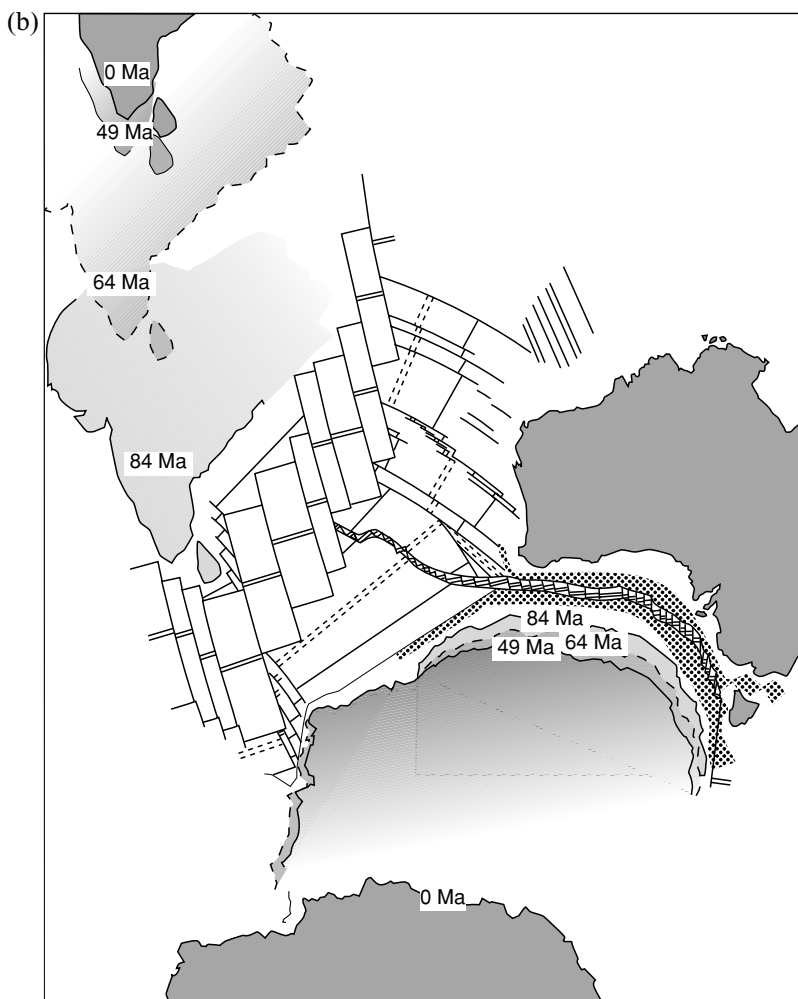


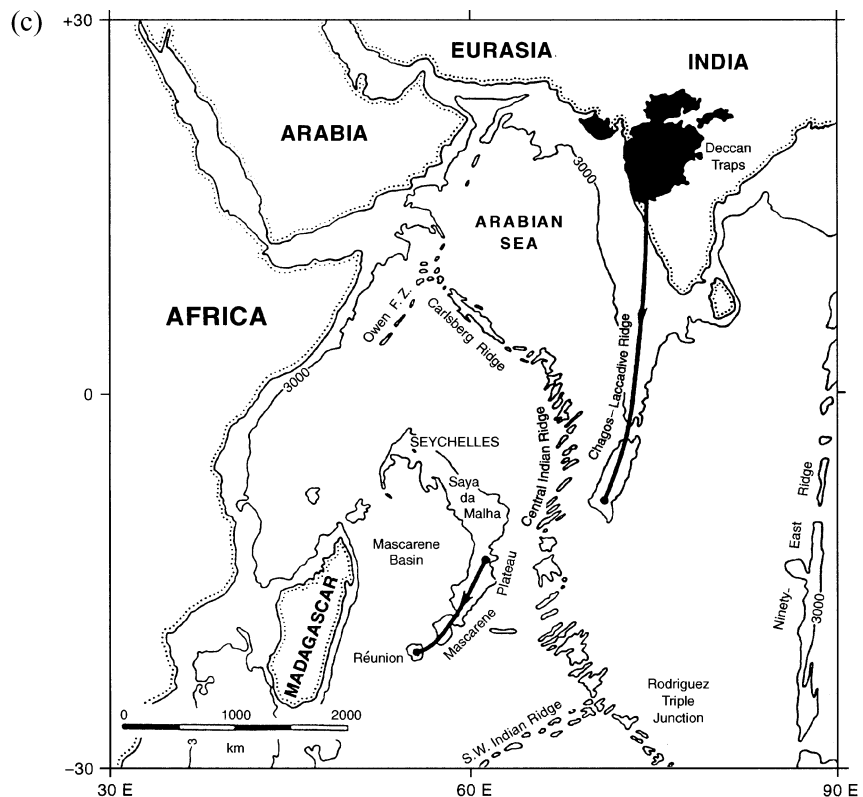
Figure 3.21. (b)
Reconstructions of the positions of India and Antarctica relative to Australia 84, 64 and 49 Ma ago. The 84-Ma mid-ocean ridge system is shown with double solid lines. The abandoned 96-Ma mid-ocean ridge system is shown with double dashed lines. The continental extension between Australia and Antarctica is stippled.
(After Powell *et al.* (1988).)

province in India. First, at about 65 Ma, the Deccan Traps⁵ were erupted in a major and sudden outpouring of lava with a total volume of well over one million cubic kilometres. Then, as India moved northwards, the hotspot formed the Chagos–Maldives–Laccadive Ridge and the Mascarene Plateau. The hotspot track was subsequently split by spreading on the Central Indian Ridge. The volcanically active Réunion Island marks the present position of the hotspot (Fig. 2.19a).

At about the time of anomaly 19 (43 Ma), there was a major reorganization in the plate motions when the Indian and Asian continents collided (refer to

⁵ The Deccan Traps, like the Paraná in Brazil (at the western end of the Rio Grande Ridge, the Tristan hotspot track) are continental flood basalts. These huge volumes of tholeiitic basalt were erupted very rapidly and were a consequence of decompression melting (sometimes called pressure-release melting) of a rising hot mantle plume head when it reached the rifting continental lithosphere.

Figure 3.21. (c) The Mascarene Plateau and the Chagos–Maldives–Laccadive Ridge mark the track of the Réunion hotspot from the initial massive outpouring of basalt in the Deccan Traps to its present location beneath Réunion Island. (After White, R. and McKenzie, D. 'Magmatism at rift zones: the generation of volcanic continental margins and flood basalts', *J. Geophys. Res.*, **94**, 7685–729. Copyright 1989 American Geophysical Union. Reproduced by permission of American Geophysical Union.)



Section 10.2.3 for details of continent–continent collisions). It is apparent in Fig. 3.20 that a second major change of spreading direction must have occurred on the Southeast Indian Ridge at this time. Older anomalies strike approximately east–west, whereas the younger anomalies strike northwest–southeast. Therefore, prior to the time of anomaly 19, the Southeast Indian Ridge was striking east–west and the east–west magnetic anomalies in the Arabian Sea, south of India and in the Bay of Bengal were all formed by the same ridge. Almost all the lineations formed on the north side of that section of the ridge which lay to the east of the Ninety-East Ridge (a hotspot trace) as well as the extinct ridge itself have been subducted by the Java Trench, the only subduction zone in the Indian Ocean. The ridge between Australia and Antarctica continued to spread very slowly. The fate of the ridge between Australia and India is not clear. It is possible that India and Australia then lay on the same plate. There has been only slight motion between India and Australia since about the time of anomaly 13. Very broad ‘diffuse’ plate boundaries subdivide the Indian plate into the Indian, Australian and Capricorn plates, with the Capricorn plate lying to the east of the Central Indian Ridge between 10°S and 30°S and extending east to ~80°E.

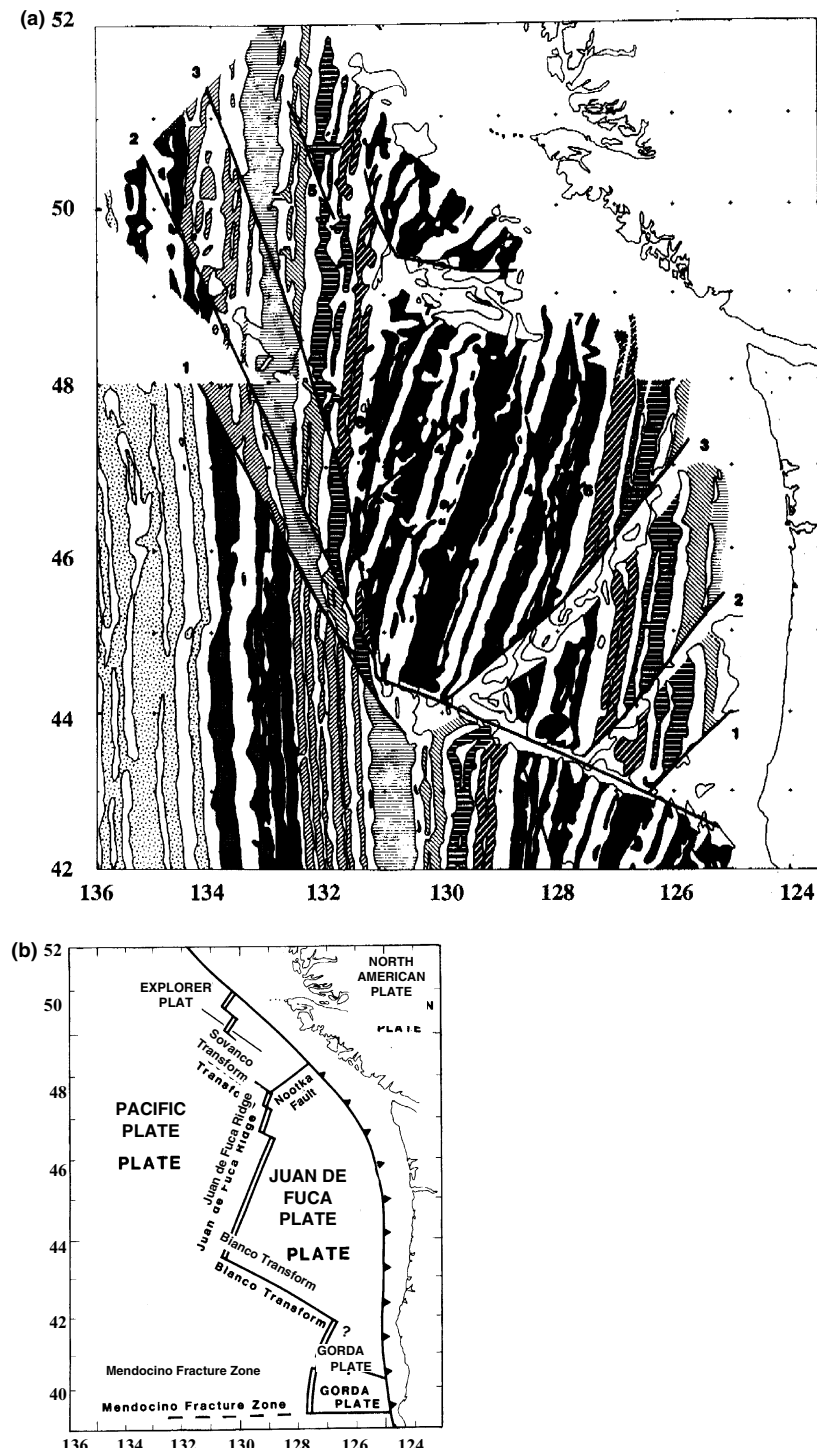
The fine details of the motions of the plates in this region and the exact positioning of the continents as they were prior to anomaly M25 when they formed the mega-continent Gondwanaland remain to be firmly established, but on a broad scale the motions are fairly well understood.

3.3.4 The Pacific Ocean

The magnetic-anomaly pattern off the west coast of North America was the first magnetic-anomaly pattern to be studied in detail (Fig. 3.7). An interpretation of these anomalies based on the plate motions and earthquakes in the area is shown in Fig. 3.22. The details of the plate boundaries and their relative motions and ages are much clearer. Although the ridges in this region are spreading relatively slowly, the plates are small, so the lithosphere was only about 10 Ma old when it was subducted beneath the North American plate. Another feature of the magnetic anomalies in this region is the difference of some 20° between the present-day trend of the Juan de Fuca Ridge and the strike of the older anomalies on the Pacific plate (the southwest part of Fig. 3.22(a)). This difference is caused by changes in the rotation pole and subsequent reorientation of the ridge. The diagonal *pseudofaults* which offset the magnetic anomalies in this region are also due to the adjustment of the ridge system to changes in the rotation poles (Fig. 3.23). Thus, when an area is studied in detail, the original questions may well be answered and theories validated, but usually new questions are also raised (in this instance, the new problem is the exact method by which ridges adjust to changes in rotation poles, or vice versa). The past plate motions in other parts of the Pacific are more difficult to interpret than those in the region flanking North America, where the presence of an active ridge system means that both sides of the anomaly pattern are preserved.

Further to the south and west on the Pacific plate, the oceanic anomaly pattern is, on a broad scale, fairly simple (Figs. 3.24 and 3.28). Anomalies strike almost north–south and are offset by fracture zones (see Section 9.5.1). The central part of the ocean was formed during a period which included the Magnetic Quiet Zone. Thus, there are not many anomalies to be observed. However, much farther north towards the Aleutian islands the pattern changes. The anomalies change direction so that they are striking approximately east–west. This feature is called the Great Magnetic Bight. The other main feature of the northern Pacific is that the north–south anomalies represent only the western half of the pattern and, except for the short ridge segments such as the Juan de Fuca Ridge, the mid-ocean ridge that created the oceanic plate no longer exists. This vanished ridge has been subducted under the North American plate. With it went much of the Farallon plate, the name given to the plate which once was to the east of the ridge and had the matching half of the symmetrical anomaly pattern (Fig. 3.24). For the Farallon plate and the Pacific–Farallon Ridge to have been subducted in this manner, the rate of subduction must have been greater than the rate at which the ridge

Figure 3.22. (a) Magnetic-anomaly data for the northeastern Pacific Ocean. Solid black lines are major offsets in the anomaly pattern (termed *pseudofaults*). This figure, which includes the data shown in Fig. 3.7, has been shaded so that the ages of the various anomalies stand out. (b) The location map for (a), showing the plates and plate boundaries. Juan de Fuca and Explorer plates are undergoing oblique subduction beneath the North American plate. There is left-lateral strike-slip motion along the Nootka fault and right-lateral strike-slip motion along the Queen Charlotte Fault (see Fig. 3.27). (After Wilson *et al.* (1984).)



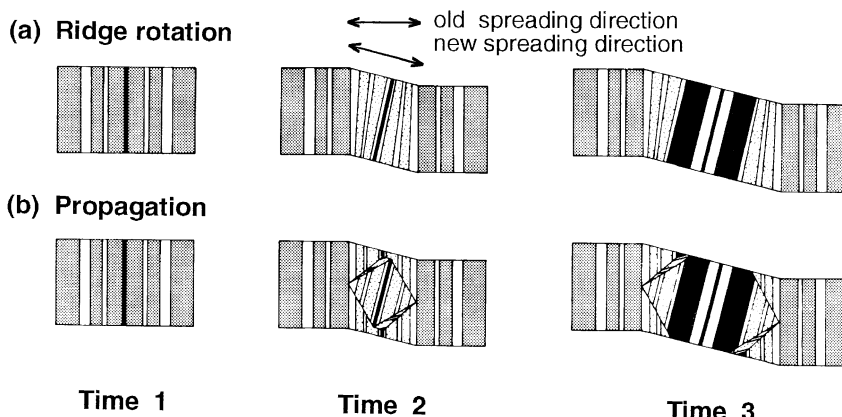


Figure 3.23. Magnetic-anomaly patterns for two possible mechanisms by which a mid-ocean ridge could adjust to changes in its spreading direction caused by a change in rotation pole. (a) Ridge rotation. In this model the spreading at the ridge is asymmetrical during the adjustment time. Half-spreading rates are not equal on both sides of the ridge and vary along the length of the ridge. (b) Propagating rifting. In this model a section of the ridge is assumed to jump to its new orientation. This 'propagating' ridge segment then lengthens and pseudofaults develop at oblique angles to the ridge as observed in Fig. 3.22(a). (From Wilson *et al.* (1984).)

was spreading. All that remains are short segments of the ridge and fragments of the Farallon plate, now the Juan de Fuca, Explorer, Gorda, Cocos and Nazca plates.

The change in direction of the magnetic anomalies in the Great Magnetic Bight region indicates that a third plate was involved (Fig. 2.16 shows that three ridges meeting at a triple junction would produce such an anomaly pattern). This third plate has been named the Kula plate. The Pacific, Farallon and Kula plates are thus assumed to have met at an RRR triple junction (the Kula Triple Junction). The spreading rates and directions of these ridges have to be determined from the anomalies and fracture zones in the vicinity of the Great Magnetic Bight. The Kula plate has been subducted beneath the North American plate and so no longer exists, although a very small piece may be trapped on the Pacific plate in the western Aleutian arc. Both the other ridges have also been subducted. Putting all of this information together to determine the motions of the plates in the northern Pacific region for the last 80 Ma involves much spherical geometry and computing. An idealized flat-plate model illustrating the main features of the evolution of the northeastern Pacific was shown in Chapter 2, Problem 2. Figure 3.25 shows a reconstruction of the evolution of this region from 50 Ma until the present time. From 80 Ma until about 55 Ma there were four plates in this northern Pacific region (North America, Kula, Farallon and Pacific). Two of them were being subducted beneath the North American plate: the Kula plate in the north and the Farallon plate farther south. About 55 Ma ago the northern

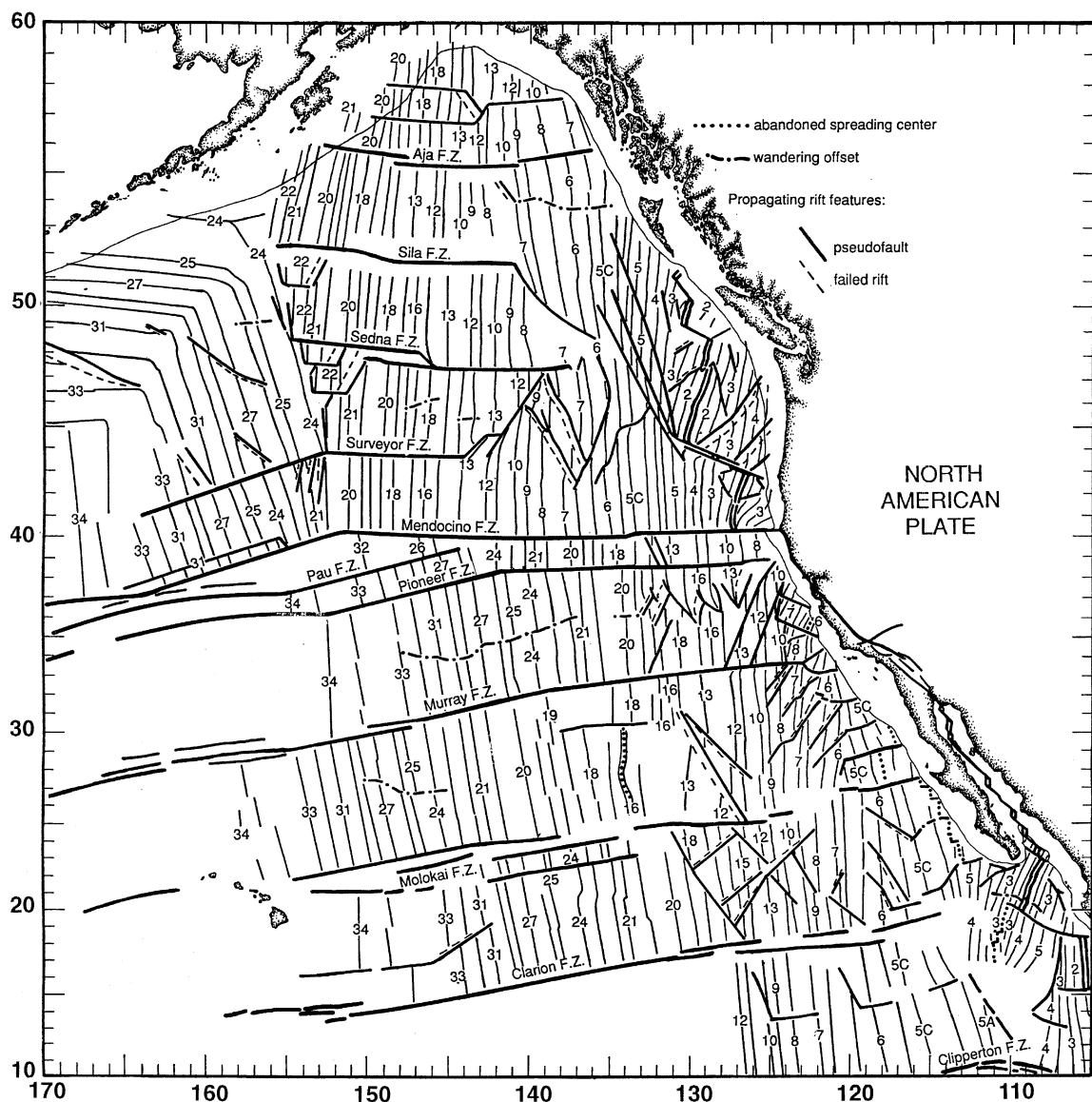


Figure 3.24. Magnetic anomalies in the northeastern Pacific. Numbers are anomaly numbers (Fig. 3.14), not ages. (From Atwater (1989).)

part of the Farallon plate broke off to form the Vancouver plate. The present Juan de Fuca plate is the remnant of this plate. The location of the boundary between the Vancouver and Farallon plates was rather variable but the relative motion was slow oblique compression and subduction of the Vancouver plate beneath North America continued to take place. At about 30 Ma, the situation changed when the ridge between the Farallon and Pacific plates first reached the

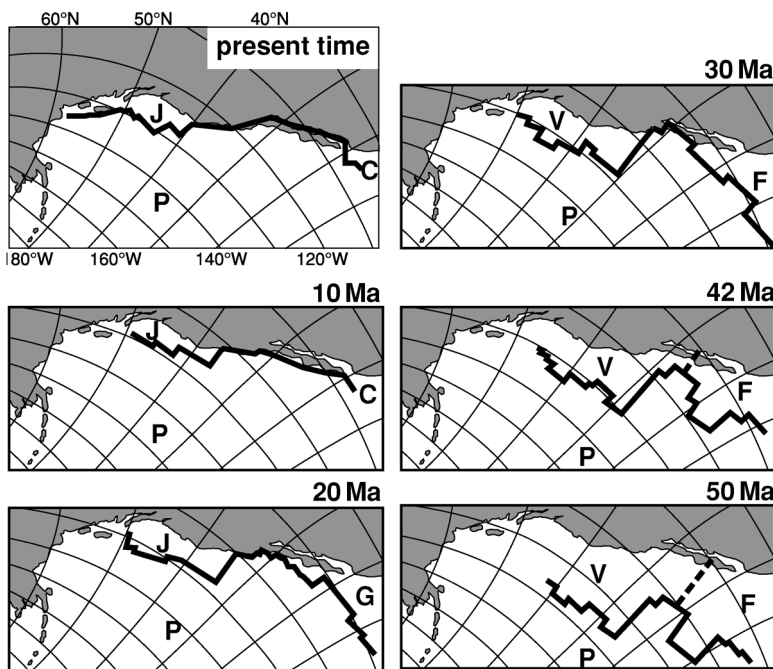


Figure 3.25. Reconstructions of the positions of the Pacific plate and the Farallon plate with respect to the North American plate (shaded). P, Pacific plate; F, Farallon plate; V, Vancouver plate; J, Juan de Fuca plate; G, Guadalupe plate; and C, Cocos plate. (From Atwater (1989), after Stock and Molnar (1988).)

subduction zone. This meant that subduction ceased on that part of the North American plate boundary where the North American plate was adjacent to the Pacific plate as the relative motion between the Pacific and North American plates was parallel to the boundary. Thus, the San Andreas Fault and the Mendocino Triple Junction were born. By 10 Ma, the Farallon–Guadalupe–Cocos plate was very small, and the San Andreas Fault system had lengthened. At about 9 Ma and 5 Ma, as discussed earlier, the strike of the Juan de Fuca Ridge changed by some 20° in total, resulting in the present configuration of the plates. The geological evolution of western North America was controlled by the motions of these oceanic plates. If the relative motion between the Pacific and North American plates is assumed to have been parallel to the subduction zone between the Farallon and North American plates (the present-day Cascadia Subduction Zone), the Mendocino Triple Junction, where the Farallon, North American and Pacific plates meet, must have been stable (Figs. 2.16, 3.26 and 3.27). However, since the Cascadia Subduction Zone is not, at present, collinear with the San Andreas Fault, the triple junction is unstable and may well always have been unstable (Fig. 3.27). The evolution of this unstable triple junction is shown in Fig. 3.26(e). If the three plates are assumed to be rigid, a hole must develop. Such a hole would presumably fill with rising mantle material from below and sediments from above. It would become in effect a microplate. Alternatively, if the continental North American plate is allowed to deform, then the triple junction evolves as shown in Fig. 3.26(f), with internal deformation involving both extension and rotation over

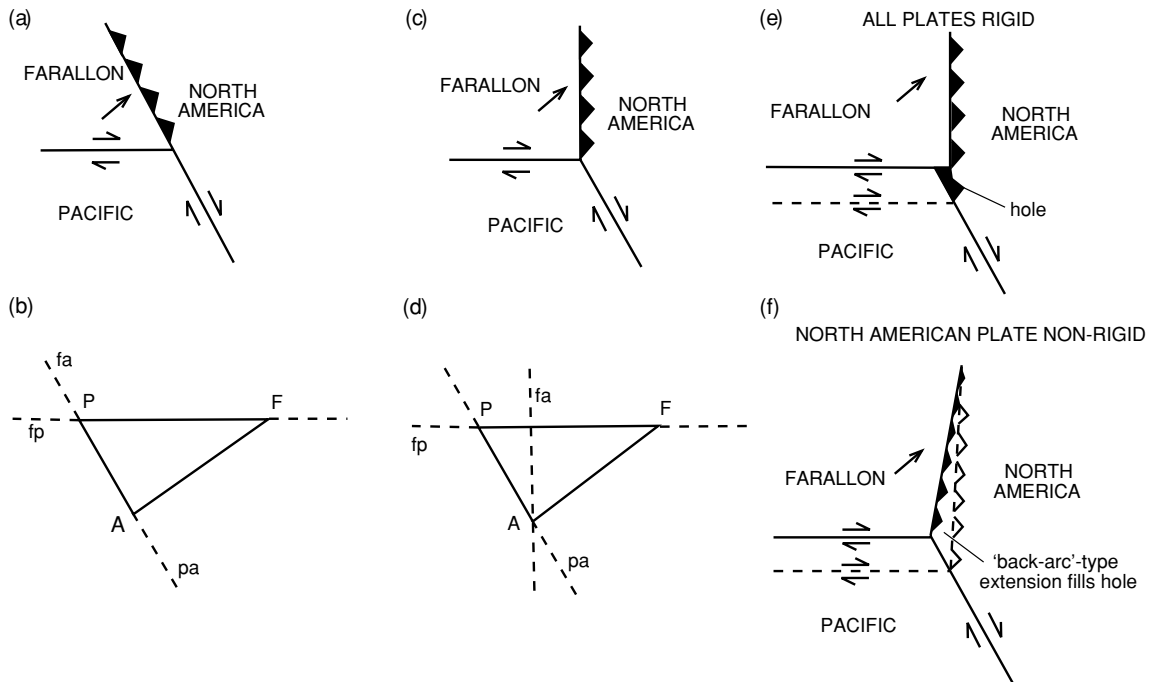


Figure 3.26. Evolution of the Mendocino Triple Junction (prior to change in Juan de Fuca rotation pole). (a) A stable Mendocino Triple Junction with the subduction zone and the fault being collinear, as in Fig. 3.25. (b) Relative-velocity vectors for the geometry in (a). (c) An unstable Mendocino Triple Junction; the subduction zone and the fault are not collinear. (d) Relative-velocity vectors for the geometry shown in (c). (e) Evolution of the triple junction shown in (c) when the three plates are assumed to be rigid. (f) Alternative evolution of the triple junction shown in (c) if the two oceanic plates are assumed to be rigid but the continental (North American) plate is allowed to deform. (From Ingersoll (1982).)

a wide zone to the east of both the subduction zone and the fault. The deformations which would be produced by this process are identical to those indicated by continental palaeomagnetic data and would account for the regional extension in the western U.S.A. (which began about 30 Ma ago when the Mendocino Triple Junction was formed), as well as for the eastward stepping of the San Andreas Fault with time, which has transferred parts of coastal California from the North American plate to the Pacific plate. This eastward stepping of the plate boundary has effectively been accomplished by the capture of sections of the partially subducted Farallon plate by the Pacific plate. This capture of subducted parts of oceanic plate subjected the overriding North American continental margin to distributed shear and extensional forces. Ultimately parts of the overriding margin joined the Pacific plate and the plate boundary stepped eastwards, with regions, such as the Western Transverse Ranges, being caused to rotate and zones of extension developing as a result. Baja California has rotated clockwise and

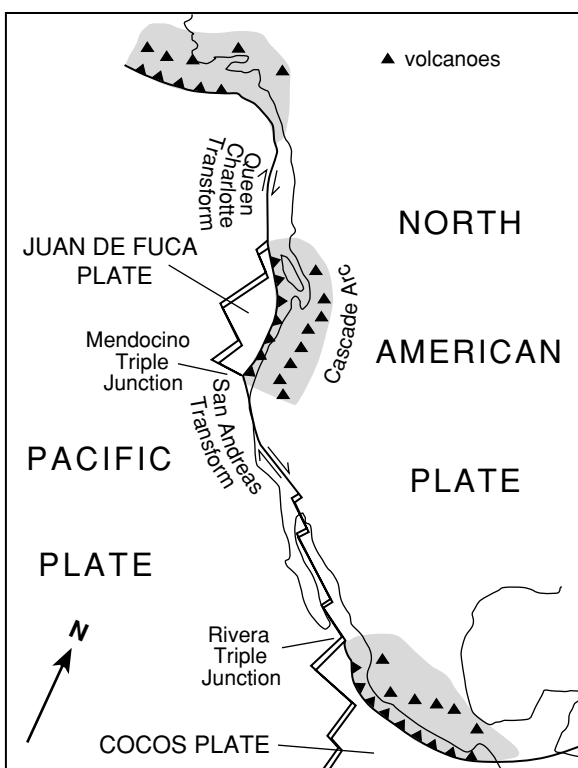


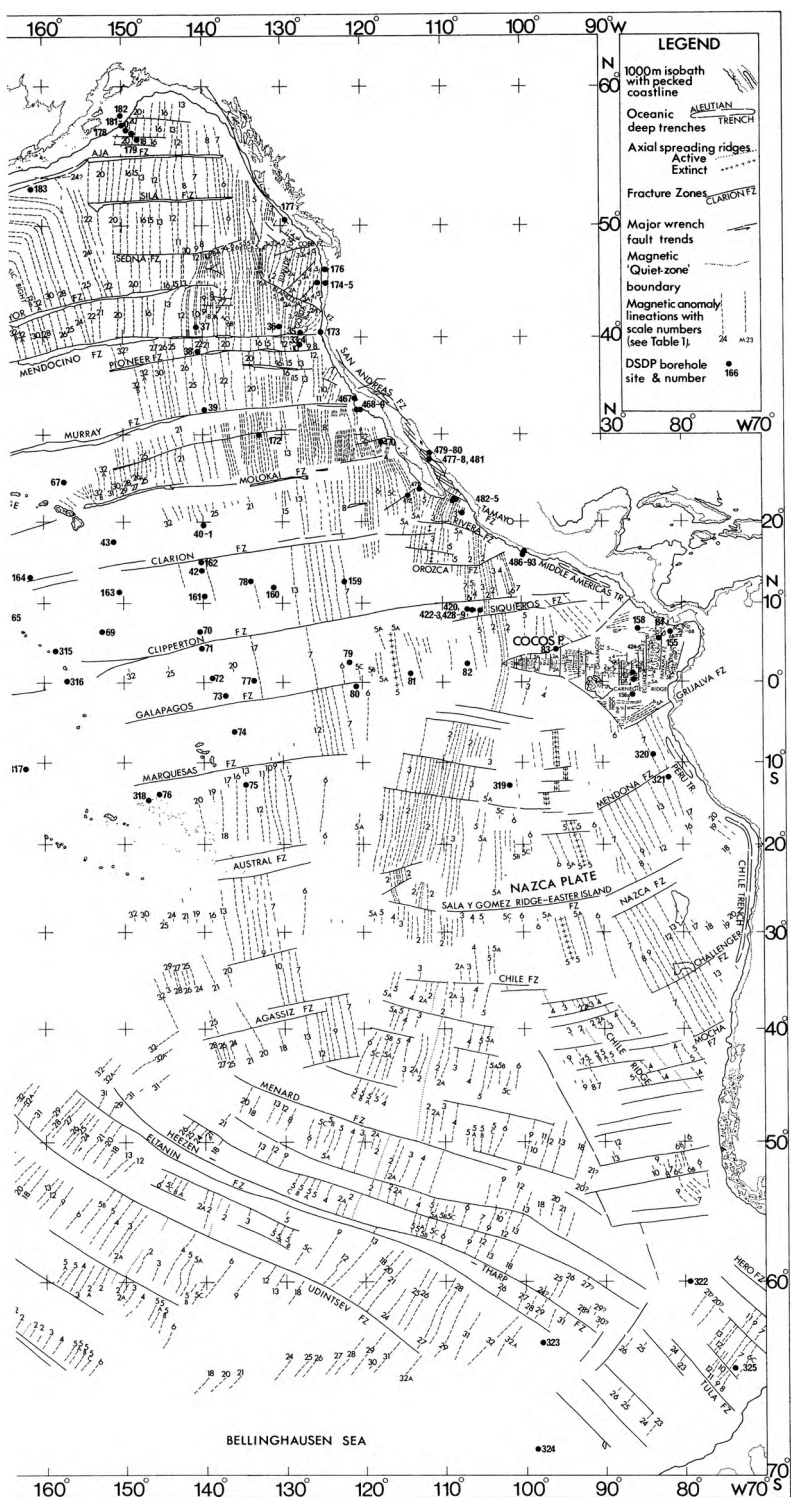
Figure 3.27. A present-day tectonic map of the western part of the North American plate. Shaded regions mark the extent of expected arc magmatism. (After Dickinson (1979).)

been translated northwards since its initial rift from North America at about 12–14 Ma. Details of the past plate motions and their effect on the interior of the North American plate will no doubt continue to be revised for many years, but the main features of the model as presented here are probably nearly correct.

Farther south, to the west of the Middle Americas Trench, magnetic lineations striking east–west are sandwiched between north–south anomalies (Fig. 3.28). This region has undergone a series of plate reorganizations since 30 Ma when the Pacific–Farallon Ridge first intersected the North American Subduction Zone. In general terms these reorganizations can best be described as the breaking up of large plates into smaller plates as the ridge was progressively subducted. At 30 Ma one plate (Farallon) lay to the east of the ridge. At 25 Ma the east–west anomalies indicate that the Cocos–Nazca Ridge (otherwise known as the Galapagos spreading centre) started spreading; so two plates, the Nazca plate and the Cocos or Guadalupe plate, lay to the east of the ridge. At about 12 Ma, the Cocos plate subdivided, spawning the tiny Rivera plate; and now three plates lie to the east of the ridge we call the East Pacific Rise (Fig. 2.2). A schematic flat model of the plates in this region was presented in Chapter 2, Problem 10.

The magnetic lineations in the northwestern Pacific region are much older and more complex than those of the northeastern Pacific (Fig. 3.28). As plates





become older, tectonic reconstructions generally become increasingly difficult and subject to error and, frequently, to speculation. The southwest–northeast lineations extending from the Japan trench towards the Aleutian trench are called the Japanese lineations. The northwest–southeast lineations to the south and west of the Emperor Seamounts and the Hawaiian Ridge are called the Hawaiian lineations. Both the Japanese and the Hawaiian lineations are identified as M1 to M29 inclusive. The east–west lineations that straddle the equator and extend from 160°E to 170°W are the Phoenix lineations (so named because of their proximity to the Phoenix Islands).

The Japanese and Hawaiian lineations form a well-defined magnetic bight, older than, but otherwise very similar to, the Great Magnetic Bight in the north-eastern Pacific. This older magnetic bight is thought to have been formed by an RRR triple junction, where the Farallon and Pacific plates met a third plate, the Izanagi plate (Fig. 3.29).

The Phoenix lineations are from anomalies M1 to M25 inclusive and were produced, between about 127 and 155 Ma, by an east–west striking Phoenix–Pacific Ridge possibly some 40° south of their present latitude. It has been suggested that this ridge extended far to the west and joined the ridge system of the Indian Ocean that gave rise to the magnetic anomalies north of the Exmouth Plateau (Section 3.3.3). Any younger lineations and the symmetrical southern half of these Phoenix lineations are no longer present here.

There are two magnetic brights in the southern Pacific, both less well defined than their northern counterparts. The first is at the eastern end of the Phoenix lineations where the lineations (M12–M4, 137–131 Ma) bend from approximately east–west to northwest–southeast. These northwest–southeast anomalies were probably produced by the Pacific–Farallon Ridge. The second magnetic bright is at about 40°S, 145°W, where anomalies 32–20 (45–70 Ma) bend from approximately southwest–northeast to northwest–southeast. Unfortunately, much of the evidence required to determine the details of these western Pacific plates and their relative motions has been swallowed by the hungry western Pacific subduction zones.

Figure 3.29 shows a series of reconstructions of the plates in the Pacific from 110 Ma to the present. The Magnetic Quiet Zone lasted from 124 to 84 Ma, so not much can be deduced about the motions of the plates during that period. The Kula plate came into existence then. It is not possible for the Kula plate to be the older Izanagi plate; rather, it is believed to have been a piece that broke off either the Farallon plate or the Pacific plate. The Farallon plate was very large indeed: between about 85 and 55 Ma ago the Pacific–Farallon Ridge extended for some 10 000 km.

The evolution of the western and southern Pacific was clearly very complex, with a number of changes in spreading centres. The process probably included the creation and subduction of whole plates. No doubt further detailed mapping of

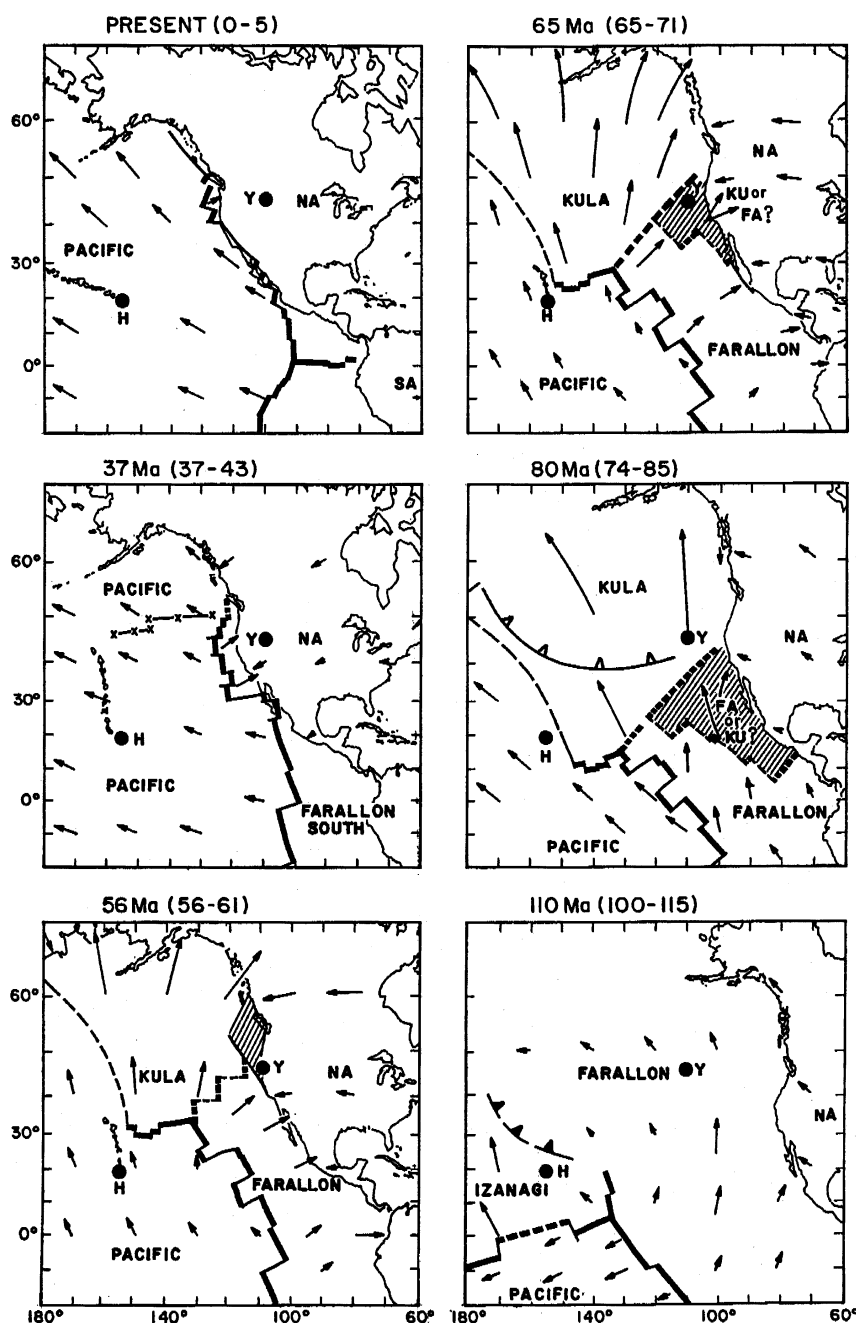


Figure 3.29.
Reconstruction of the motions of the Pacific, Izanagi, Farallon, Kula and North American (NA) plates. Arrows indicate motion of the plates with respect to the hotspots. The hatched region at 56–80 Ma indicates the range of possible locations for the ridge between the Kula and Farallon plates. Y, Yellowstone hotspot; and H, Hawaiian hotspot. (From Atwater (1989).)

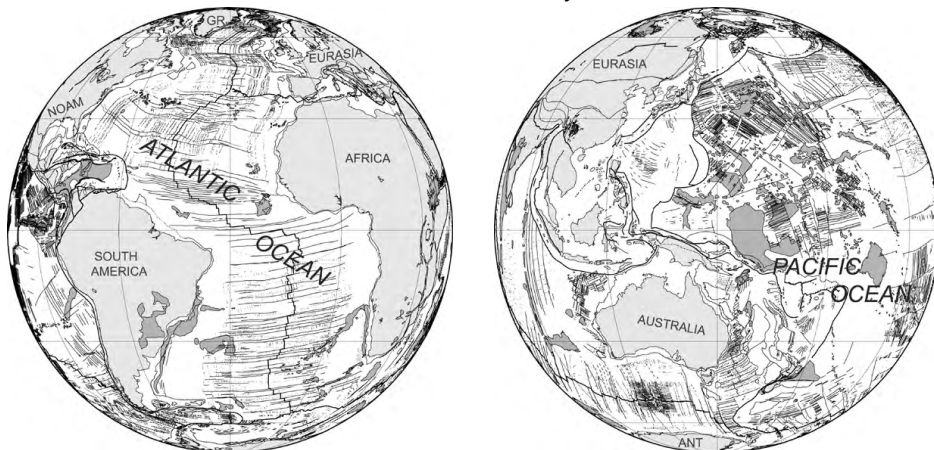
the seafloor, the lineations, palaeomagnetic measurements and dating of drilled and dredged basement samples will slowly refine and improve the picture of the history of the Pacific back to Jurassic time.

3.3.5 The continents

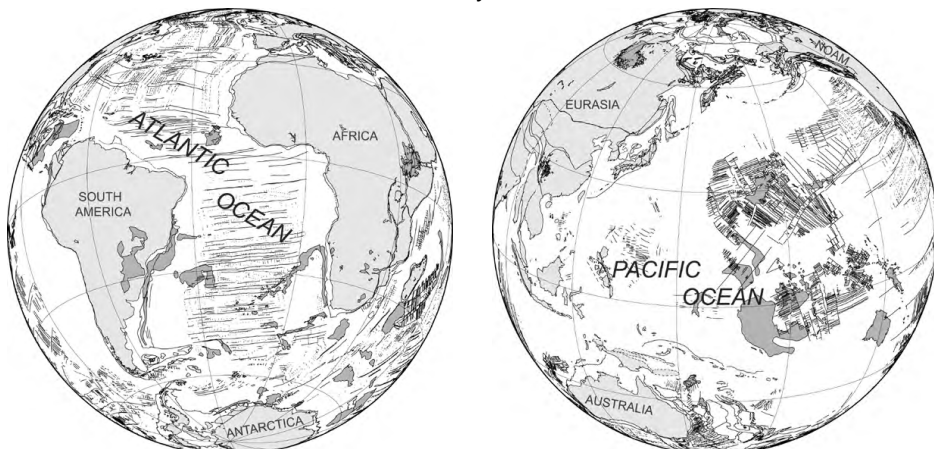
Figure 3.30, a series of snapshots of the continents, shows how they have moved relative to each other through the Phanerozoic. By the late Carboniferous to earliest Permian, the continents were all joined together and formed one supercontinent, which we call *Pangaea* (Greek, ‘all lands’). The northern part of Pangaea, comprising today’s North America, Greenland and Eurasia, has been named *Laurasia* or *Laurentia*, and the southern part of the continent, comprising South America, Africa, India, Antarctica and Australia, is called *Gondwanaland*. Laurasia and Gondwanaland became distinct during the Jurassic when Pangaea rifted in two. The wedge-shaped ocean between Laurasia and Gondwanaland is the *Tethys* Sea. (*Tethys* was the wife of Oceanus in Greek mythology.) It is this sea which has presumably been subducted beneath Laurasia as India and Africa have moved northwards. The Mediterranean, Caspian and Black Seas are the last vestiges of this ancient ocean, the completion of whose subduction resulted in the building of the Alpine, Carpathian and Himalayan mountain chains. All these regions contain scattered outcrops of ophiolites (a suite of rocks with chemical and lithological similarities to the oceanic crust, which may be examples of crust from ancient back-arc basins, Section 9.2.1). There is considerable current debate about the reconstruction of continental fragments prior to the Pangaea supercontinent (uncertainty increases with age) and there are many differing views on the arrangements of the current continental pieces into pre-Pangaean supercontinents. Rodinia was a Mid-to-Late Proterozoic (750–~1000 Ma) supercontinent. It is proposed that, in the Late Proterozoic, it broke up into Pannotia, Siberia and North China. Pannotia then further split into Laurentia (the Precambrian core of North America), Gondwanaland and Baltica. It is proposed that, at about the same time, there was a major global glaciation (‘snowball’ Earth). The oldest reconstructions shown in Fig. 3.30, which are largely based on Dalziel (1997), are presented only as one example of what Precambrian geography may have been like, rather than as absolute fact.

Figure 3.30. Palaeocontinental maps showing the present-day continents in their previous positions. ANT, Antarctica; GR, Greenland; IND, India; M, Madagascar; NOAM, North America; and SOAM, South America. Solid lines, fracture zones and magnetic lineations. Dark grey shading, large igneous provinces (LIPs) volcanics produced at hot spots. (Reconstructions provided by Kylara Martin of the PLATES Project, Institute for Geophysics, University of Texas at Austin, Lawver *et al.* 2003.)

0 Ma Present Day



20 Ma Early Miocene



40 Ma Middle Eocene

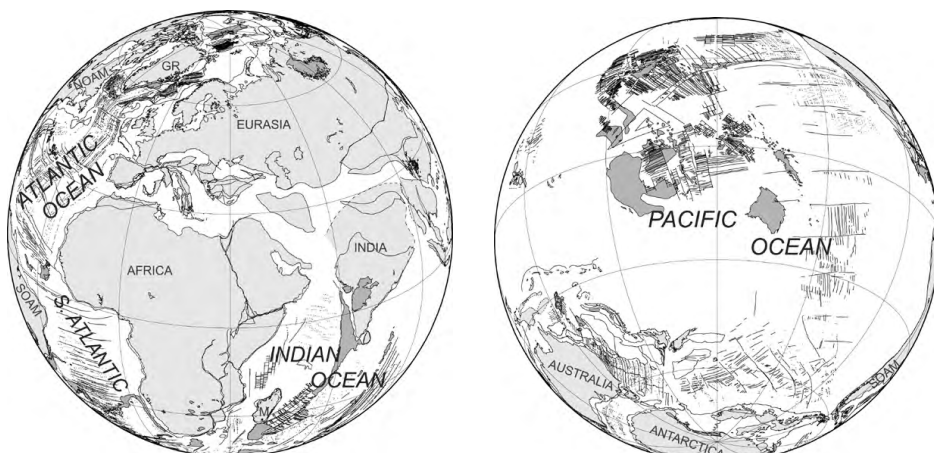


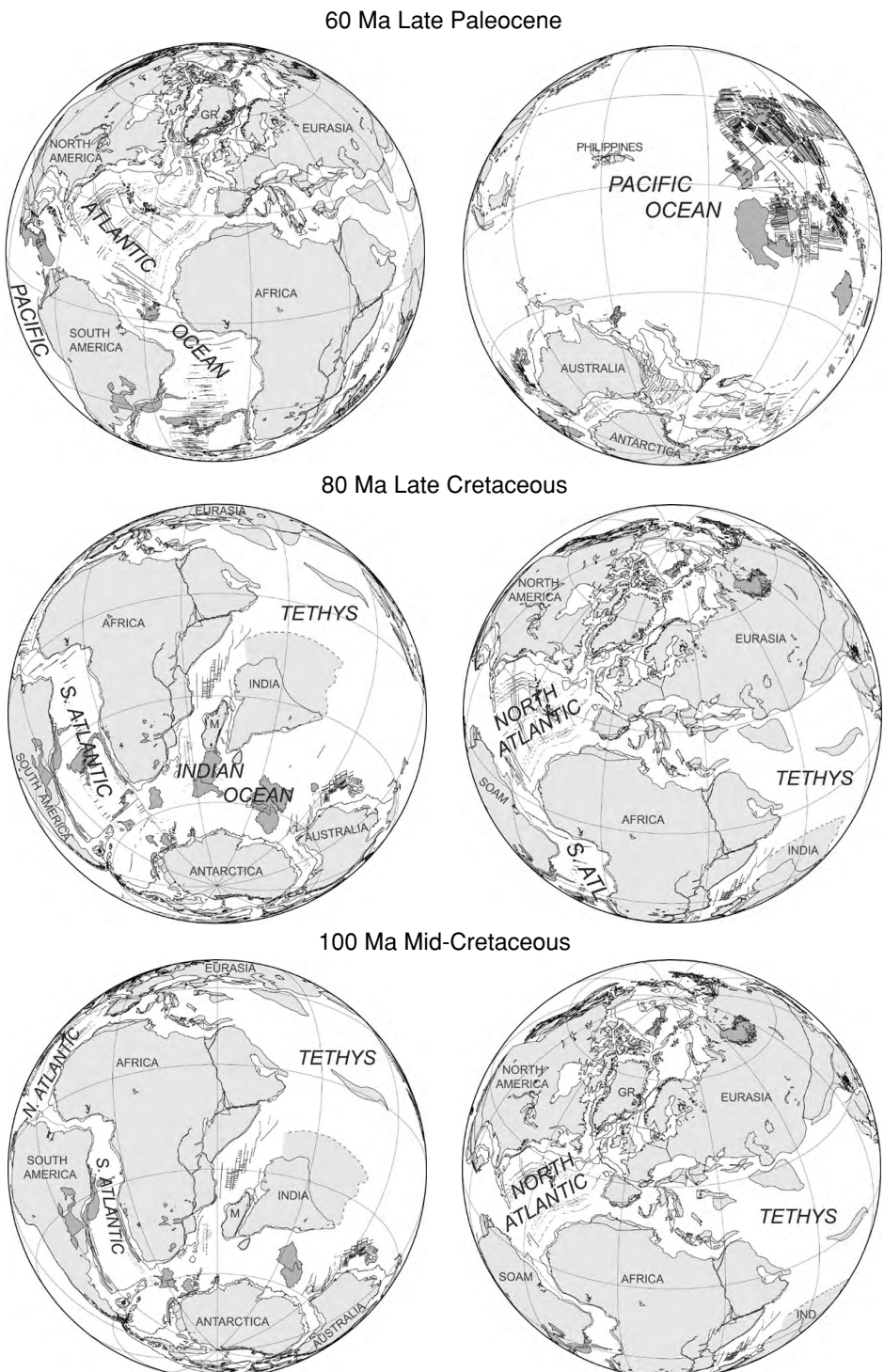
Figure 3.30. (cont.)

Figure 3.30. (cont.)

125 Ma Early Cretaceous

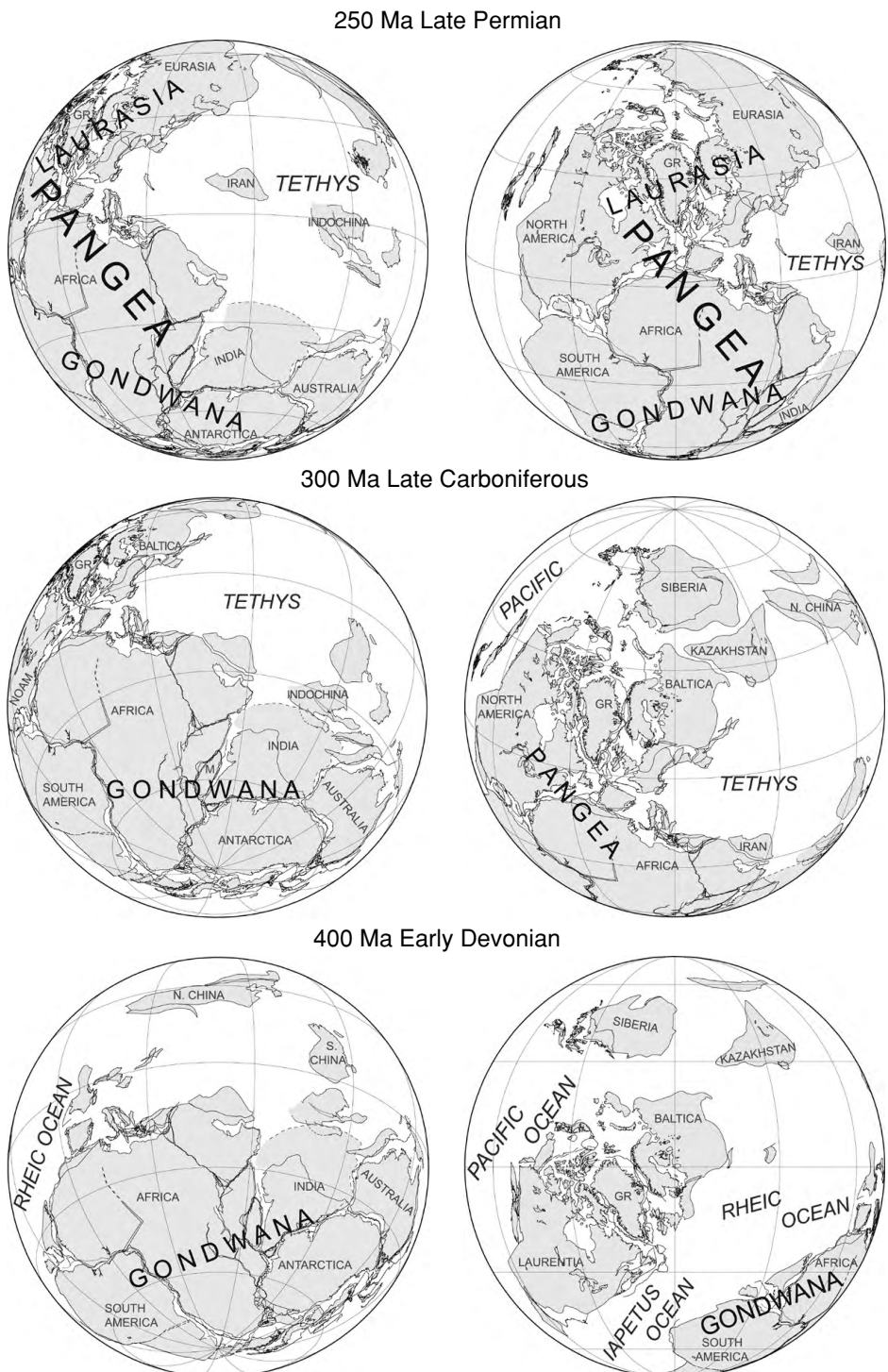


150 Ma Late Jurassic



200 Ma Early Jurassic



Figure 3.30. (cont.)

550 Ma Early Cambrian

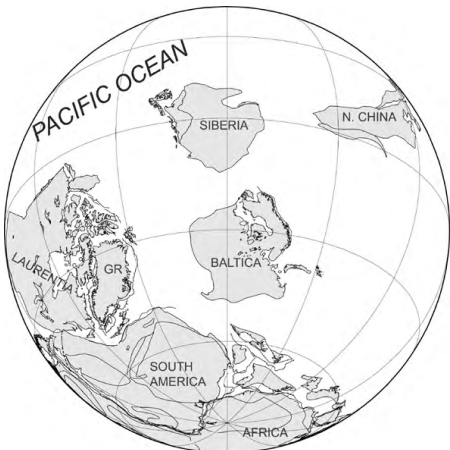


Figure 3.30. (cont.)



725 Ma Late Proterozoic



Problems

1. Assume that the Earth's magnetic field is a dipole aligned along the geographic north–south axis.
 - (a) What is the angle of inclination at London, U.K. (51°N , 0°E)?
 - (b) What is the angle of inclination at Canberra, Australia (35°S , 149°E)?
 - (c) What is the angle of inclination on Spitzbergen (78°N , 16°E)?
 - (d) What is the angle of inclination at Rio de Janeiro, Brazil (23°S , 43°W)?
 - (e) If the angle of inclination is 76° , where are you?
 - (f) If the angle of inclination is -36° , where are you?
2. Magnetic measurements have been made on some lavas found at 60°N , 90°W . The angle of inclination is measured to be 37° . At what magnetic latitude were these lavas erupted?

3. If the direction of magnetization of the lavas of Problem 2 is due west, calculate the position of the pole of the Earth's magnetic field at the time the lavas were erupted. What does this indicate about the continent on which these lavas occur?
4. If the measurement of the angle of inclination of the lavas of Problem 2 is in error by 5° , what is the subsequent error in the calculated palaeolatitude?
5. Down to what depth can (a) oceanic lithosphere and (b) continental lithosphere be permanently magnetized? (Hint: see Chapter 7.)
6. (a) Use Fig. 3.12 to calculate a spreading rate for the South Atlantic. Is this a half-spreading rate or a plate-separation rate?
 (b) Using Fig. 3.12, estimate minimum and maximum spreading rates for the Pacific during the last 80 Ma.
7. Calculate the minimum length of time that a reversal of the Earth's magnetic field lasted if it was detected from sea-surface magnetic data collected in (a) the Atlantic Ocean and (b) the equatorial Pacific Ocean.
8. Where is the oldest ocean floor, and what age is it? Discuss what may have happened to the rest of the ocean floor of this age and why.
9. At any given latitude, what orientation of ridge gives rise to the largest-amplitude magnetic anomalies?
10. At what latitude do magnetic anomalies due to magnetized oceanic crust have minimum amplitude?

References and bibliography

- Atwater, T. 1970. Implications of plate tectonics for the Cenozoic tectonic evolution of western North America. *Bull. Geol. Soc. Am.*, **81**, 3513–36.
1989. Plate tectonic history of the northeast Pacific and western North America. In E. L. Winterer, D. M. Hussong and R. W. Decker, eds., *The Geology of North America, Vol. N, The Eastern Pacific Ocean and Hawaii*. Boulder, Colorado: Geological Society of America, pp. 21–7.
- Atwater, T. and Severinghaus, J. 1989. Tectonic maps of the northeast Pacific. In E. L. Winterer, D. M. Hussong and R. W. Decker, eds., *The Geology of North America, Vol. N, The Eastern Pacific Ocean and Hawaii*. Boulder, Colorado: Geological Society of America, pp. 15–20.
- Bambach, R. K., Scotese, C. R. and Ziegler, A. M. 1980. Before Pangea: the geographies of the Paleozoic world. *Am. Sci.*, **68**, 26–38.
- Barton, C. E. 1996. Revision of International Geomagnetic Reference Field released. *EOS Trans. Am. Geophys. Un.*, **77** (16), 153.
1997. International Geomagnetic Reference Field: the seventh generation. *J. Geomag. Geoelectr.*, **49**, 123–48.
- Briden, J. C., Hurley, A. M. and Smith, A. G. 1981. Paleomagnetism and Mesozoic–Cenozoic paleocontinental world maps. *J. Geophys. Res.*, **86**, 11 631–56.
- Brunhes, B. 1906. Recherches sur la direction d'aimantation des roches volcaniques (1). *J. Physique, 4ième Sér.*, **5**, 705–24.
- Bullard, E. C. and Mason, R. G. 1963. The magnetic field over the oceans. In M. N. Hill, ed., *The Sea*, Vol. 3. New York: Wiley, pp. 175–217.

- Candé, S. C. and Kent, D. V. 1992. A new geomagnetic polarity timescale for the Late Cretaceous and Cenozoic. *J. Geophys. Res.*, **97**, 13 917–51.
1995. Revised calibration of the geomagnetic polarity timescale for the Late Cretaceous and Cenozoic. *J. Geophys. Res.*, **100**, 6093–5.
- Candé, S. C. and Mutter, J. C. 1982. A revised identification of the oldest sea-floor spreading anomalies between Australia and Antarctica. *Earth Planet. Sci. Lett.*, **58**, 151–60.
- Dalziel, I. W. D. 1997. Neoproterozoic–Paleozoic geography and tectonics: review, hypothesis, environmental speculation. *Geol. Soc. Am. Bull.*, **109** (1), 16–42.
- DeMets, C. and Royer, J.-Y. 2003. A new high-resolution model for India–Capricorn motion since 20 Ma: implications for chronology and magnitude of distributed crustal deformation in the Central Indian Basin. *Current Sci.*, **85**, 339–45.
- Dickinson, W. R. 1979a. Cenozoic plate tectonic setting of the Cordilleran region in the United States. In J. M. Armentrout, M. R. Cole and H. TerBest Jr, eds., *Cenozoic Paleogeography of the Western United States*. Pacific Coast Paleogeography Symposium 3. Tulsa, Oklahoma: Society of Economic Palaeontologists and Mineralogists, pp. 1–13.
- 1979b. Plate tectonic evolution of North Pacific Rim. In S. Uyeda, R. Murphy and K. Kobayashi, eds., *Geodynamics of Western Pacific, Advances in Earth and Planetary Sciences*, 6. Tokyo: Centre for Academic Publications, pp. 1–19.
- Ellis, R. M. et al. 1983. The Vancouver Island Seismic Project: a COCRUST onshore–offshore study of a convergent margin. *Can. J. Earth Sci.*, **20**, 719–41.
- Engebretson, D. C., Cox, A. and Gordon, R. G. 1985. *Relative Motion between Oceanic and Continental Plates in the Pacific Basin*. Geological Society of America Special Paper 206. Boulder, Colorado: Geological Society of America.
- Falvey, D. A. and Mutter, J. C. 1981. Regional plate tectonics and evolution of Australia's passive continental margins. *Bur. Miner. Resour. J. Aust. Geol. Geophys.*, **6**, 1–29.
- Farrar, E. and Dixon, J. M. 1981. Early Tertiary rupture of the Pacific plate: 1700 km of dextral offset along the Emperor Trough–Line Islands lineament. *Earth Planet. Sci. Lett.*, **53**, 307–22.
- Fisher, R. L. and Goodwillie, A. M. 1997. The physiography of the Southwest Indian Ridge. *Marine Geophys. Res.*, **19**, 451–5.
- Fisher, R. L. and Sclater, J. G. 1983. Tectonic evolution of the southwest Indian Ocean ridge system since the mid-Cretaceous: plate mobility and stability of the pole of Antarctica/Africa for at least 80 My. *Geophys. J. Roy. Astr. Soc.*, **73**, 553–76.
- Gahagan, L. M. et al. 1988. Tectonic map of the ocean basins from satellite altimetry data. *Tectonophysics*, **155**, 1–26.
- Garland, D. G. 1979. *Introduction to Geophysics: Mantle, Core and Crust*, 2nd edn. Philadelphia: Saunders.
- Gilbert, W. 1600. *De magnete* (English translation by P. F. Mottelay, 1893, New York: Dover Books Inc.)
- Gradstein, F. M., Ogg, J. G. and Smith, A. G. 2004. *A Geologic Time Scale*. Cambridge: Cambridge University Press.
- Grantz, A., Johnson, L. and Sweeney, J. F., eds., 1990. *The Arctic Ocean Region, The Geology of North America*, Vol. L. Boulder, Colorado: Geological Society of America.
- Handschoen, D. W. 1976. Post-Eocene plate tectonics of the Eastern Pacific. In G. H. Sutton et al., eds., *The Geophysics of the Pacific Ocean Basin and its Margin*. Vol. 19 of

- Geophysical Monographs of the American Geophysical Union. Washington: American Geophysical Union, pp. 177–202.
- Harland, W. B., Cox A. V., Llewellyn, P. G., Pickton, C. A. G., Smith, A. G. and Walters, R. 1990. *A Geologic Time Scale 1989*. Cambridge: Cambridge University Press.
- Harrison, C. G. A. 1987. Marine magnetic anomalies – the origin of the stripes. *Ann. Rev. Earth Planet. Sci.*, **15**, 505–43.
- Heirtzler, J. R., Dickson, G. O., Herron, E. M., Pitman III, W. C. and Le Pichon, X. 1968. Marine magnetic anomalies, geomagnetic field reversals and motions of the ocean floor and continents. *J. Geophys. Res.*, **73**, 2119–36.
- Hilde, T. W. C., Isezaki, N. and Wageman, J. M. 1976. Mesozoic sea-floor spreading in the North Pacific. In G. H. Sutton *et al.*, eds., *The Geophysics of the Pacific Ocean Basin and its Margin*. Vol. 19 of Geophysical Monographs of the American Geophysical Union. Washington: American Geophysical Union, pp. 205–26.
- Hutton, V. R. S. 1976. The electrical conductivity of the Earth and planets. *Rep. Prog. Phys.*, **39**, 487–572.
- Ingersoll, R. V. 1982. Triple-junction instability as cause for late Cenozoic extension and fragmentation of the western United States. *Geology*, **10**, 621–4.
- Irving, E. 1983. Fragmentation and assembly of the continents, mid-Carboniferous to present. *Geophys. Surveys*, **5**, 299–333.
1988. The paleomagnetic confirmation of continental drift. *EOS Trans. Am. Geophys. Un.*, **69** (44), 994–1014.
- Irving, E. and Sweeney, J. F. 1982. Origin of the Arctic Basin. *Trans. Roy. Soc. Canada, Ser. IV*, **20**, 409–16.
- Klitgord, K. D. and Mammerickx, J. 1982. Northern East Pacific Rise: magnetic anomaly and bathymetric framework. *J. Geophys. Res.*, **87**, 6725–50.
- Klitgord, K. D. and Schouten, H. 1986. Plate kinematics of the Central Atlantic. In P. R. Vogt and B. E. Tucholke, eds., *The Geology of North America, Vol. M, The Western North Atlantic Region*. Boulder, Colorado: Geological Society of America, pp. 3351–78.
- Larson, R. L. and Chase, C. G. 1972. Late Mesozoic evolution of the western Pacific Ocean. *Bull. Geol. Soc. Am.*, **83**, 3627–44.
- Lawver, L. A., Sclater, J. G. and Meinke, L. 1985. Mesozoic and Cenozoic reconstructions of the South Atlantic. *Tectonophysics*, **114**, 233–54.
- Lawver, L. A., Dalziel, I. W. D., Gahagan, L. M., Martin, K. M. and Campbell, D. A. 2003. The PLATES 2003 Atlas of Plate Reconstruction (750 Ma to Present Day). PLATES Progress Report No. 280-0703. University of Texas Institute for Geophysics Technical Report No. 190. Houston, Texas: University of Texas Press.
- Lemaux II, J., Gordon, R. G. and Royer, J.-Y. 2002. Location of the Nubia–Somalia boundary along the Southwest Indian Ridge. *Geology*, **30**, 339–42.
- Malin, S. R. C. and Bullard, E. 1981. The direction of the Earth's magnetic field at London, 1570–1975. *Phil. Trans. Roy. Soc. A*, **299**, 357–423.
- Mammerickx, J. and Klitgord, K. D. 1982. Northern East Pacific Rise: evolution from 25 mybp to the present. *J. Geophys. Res.*, **87**, 6751–9.
- Matuyama Motonori 1929. On the direction of magnetisation of basalt in Japan, Tyōsen and Manchuria. *Japan Academy Proc.*, **5**, 203–5.
- Maxwell, A. E., Von Herzen, R. P., Hsü, K. J., Andrews, J. E., Saito, T., Percival Jr, S. F., Milow, E. D. and Boyce, R. E. 1970. Deep sea drilling in the South Atlantic. *Science*, **168**, 1047–59.

- McDougall, I., Brown, F. H., Cerling, T. E., and Hillhouse, J. W. 1992. A reappraisal of the geomagnetic time scale to 4 Ma using data from the Turkana Basin, East Africa. *Geophys. Res. Lett.*, **19**, 2349–52.
- McElhinny, M. W. 1973. *Palaeomagnetism and Plate Tectonics*. Cambridge: Cambridge University Press.
- McKenzie, D. P. 1973. The evolution of the Indian Ocean. *Sci. Am.*, **228** (5), 62–72.
- McKenzie, D. P. and Sclater, J. G. 1971. The evolution of the Indian Ocean since the late Cretaceous. *Geophys. J. Roy. Astr. Soc.*, **25**, 437–528.
- Molnar, P., Pardo-Casas, F. and Stock, J. 1988. The Cenozoic and late Cretaceous evolution of the Indian Ocean Basin: uncertainties in the reconstructed positions of the Indian, African and Antarctic plates. *Basin Res.*, **1**, 23–40.
- Morel, P. and Irving, E. 1981. Paleomagnetism and the evolution of Pangaea. *J. Geophys. Res.*, **86**, 1858–72.
- Morley, L. W. and Larochelle, A. 1964. Paleomagnetism as a means of dating geological events. In F. F. Osborne, ed., *Geochronology in Canada*. Royal Society of Canada Special Publication No. 8. Toronto: Toronto University Press, pp. 39–51.
- Müller, R. D., Gaina, C., Roest, W., Clark, S. P. and Sdrolias, M. 2002. The evolution of global oceanic crust from Jurassic to present day: a global data integration. In *American Geophysical Union Fall Meeting Abstracts*. Washington: American Geophysical Union.
- Müller, R. D. et al. 1997. Digital isochrons of the world's ocean floor. *J. Geophys. Res.* **102**, 3211–14.
- Mutter, J. C., Hegarty, K. A., Candé, S. C. and Weissel, J. K. 1985. Breakup between Australia and Antarctica: a brief review in the light of new data. *Tectonophysics*, **114**, 255–79.
- Ness, G., Levi, S. and Couch, R. 1980. Marine magnetic anomaly timescales for the Cenozoic and late Cretaceous: a précis, critique and synthesis. *Rev. Geophys. Space Phys.*, **18**, 753–70.
- Nicholson, C., Sorlien, C. C., Atwater, T., Crowell, J. C. and Luyendyk, B. P. 1994. Microplate capture, rotation of the Western Transverse Ranges, and initiation of the San Andreas transform as a low angle fault system. *Geology*, **22**, 491–5.
- Norton, I. O. and Sclater, J. G. 1979. A model for the evolution of the Indian Ocean and the breakup of Gondwanaland. *J. Geophys. Res.*, **84**, 6803–30.
- Ogg, J. G. 1995. Magnetic polarity time scale of the Phanerozoic. In T. J. Ahrens, ed., *Global Earth Physics: A Handbook of Physical Constants*. Washington: American Geophysical Union, pp. 240–70.
- Owen, H. G. 1983. *Atlas of Continental Displacement: 200 Million Years to the Present*. Cambridge: Cambridge University Press.
- Parkinson, W. D. 1983. *Introduction to Geomagnetism*. Edinburgh: Scottish Academic Press.
- Peddie, N. W. 1982. IGRF 1980: a report by IAGA Division Working Group 1. *Geophys. J. Roy. Astr. Soc.*, **68**, 265–8.
- Pitman III, W. C. and Heirtzler, J. R. 1966. Magnetic anomalies over the Pacific–Antarctic ridge. *Science*, **154**, 1164–71.
- Powell, C. McA., Roots, S. R. and Veevers, J. J. 1988. Pre-breakup continental extension in East Gondwanaland and the early opening of the eastern Indian Ocean. *Tectonophysics*, **155**, 261–83.
- Raff, A. D. and Mason, R. G. 1961. Magnetic survey off the west coast of North America, 40°N latitude to 50°N latitude. *Geol. Soc. Am. Bull.*, **72**, 1267–70.

- Richards, M. A., Gordon, R. G. and van der Hilst, R. D. eds. 2000. *The History and Dynamics of Global Plate Motions*. Geophysical Monograph 121. Washington: American Geophysical Union.
- Royer, J.-Y. and Gordon, R. G. 1997. The motion and boundary between the Capricorn and Antarctic plates. *Science*, **277**, 1268–74.
- Royer, J.-Y., Sclater, J. G. and Sandwell, D. T. 1989. A preliminary tectonic chart of the Indian Ocean. *Proc. Indian Acad. Sci., Earth, Planet Sci.*, **98**, 7–24.
- Schouten, H. and Denham, C. R. 1979. Modelling the oceanic source layer. In M. Talwani, G. C. A. Harrison and D. E. Hayes, eds., *Implications of Deep Drilling Results in the Atlantic Ocean: Ocean Crust*. Vol. 2 of Maurice Ewing Series. Washington: American Geophysical Union, pp. 151–9.
- Schouten, H., Denham, C. and Smith, W. 1982. On the quality of marine magnetic anomaly sources and sea floor topography. *Geophys. J. Roy. Astr. Soc.*, **70**, 245–59.
- Schouten, J. A. 1971. A fundamental analysis of magnetic anomalies over oceanic ridges. *Mar. Geophys. Res.*, **1**, 111–44.
- Sclater, J. G., Fischer, R. L., Patriat, P., Tapscott, C. and Parsons, B. 1981. Eocene to recent development of the southwest Indian ridge, a consequence of the evolution of the Indian Ocean triple junction. *Geophys. J. Roy. Astr. Soc.*, **64**, 587–604.
- Sclater, J. G., Jaupart, C. and Galson, D. 1980. The heat flow through oceanic and continental crust and the heat loss of the Earth. *Rev. Geophys. Space Phys.*, **18**, 269–311.
- Sclater, J. G., Parsons, B. and Jaupart, C. 1981. Oceans and continents: similarities and differences in the mechanisms of heat loss. *J. Geophys. Res.*, **86**, 11 535–52.
- Scotese, C. R. 1984. An introduction to this volume: Paleozoic paleomagnetism and the assembly of Pangea. In R. Van der Voo, C. R. Scotese and N. Bonhommet, eds., *Plate Reconstruction from Paleozoic Paleomagnetism*. Geodynamics Series, Vol. 12. Washington: American Geophysical Union, pp. 1–10.
- Scotese, C. R. and Sager, W. W., eds., 1988. Mesozoic and Cenozoic plate reconstructions. *Tectonophysics*, **155**.
- Smith, A. G., Hurley, A. M. and Briden, J. C. 1981. *Phanerozoic Paleocontinental World Maps*. Cambridge: Cambridge University Press.
- Spell, T. L. and McDougall, I. 1992. Revisions to the age of the Brunhes–Matuyama boundary and the Pleistocene geomagnetic polarity timescale. *Geophys. Res. Lett.*, **19**, 1181–4.
- Stein, S. and Freymuller, J. T. eds. 2002. *Plate Boundary Zones*. Geodynamics Series 30. Washington: American Geophysical Union.
- Stock, J. and Molnar, P. 1988. Uncertainties and implications of the Late Cretaceous and Tertiary position of the North American relative to Farallon, Kula and Pacific plates. *Tectonics*, **8**, 1359–70.
- Stock, J. M. and Hodges, K. V. 1989. Transfer of Baja California to the Pacific Plate. *Tectonics*, **8**, 99–115.
- Tivey, M. A. and Tucholke, B. E. 1998. Magnetization of 0–29 Ma ocean crust on the Mid-Atlantic Ridge. *J. Geophys. Res.*, **103**, 17 807–26.
- Van der Voo, R., Peinado, J. and Scotese, C. R. 1984. A paleomagnetic reevaluation of Pangea reconstructions. In R. Van der Voo, C. R. Scotese and N. Bonhommet, eds., *Plate Reconstruction from Paleozoic Paleomagnetism*. Geodynamics Series, Vol. 12. Washington: American Geophysical Union, pp. 11–26.

- Veevers, J. J. 1984. *Phanerozoic Earth History of Australia*. Oxford: Clarendon.
1986. Breakup of Australia and Antarctica estimated as mid-Cretaceous (95 ± 5 Ma) from magnetic and seismic data at the continental margin. *Earth Planet. Sci. Lett.*, **77**, 91–9.
- Vine, F. J. 1966. Spreading of the ocean floor: new evidence. *Science*, **154**, 1405–15.
- Vine, F. J. and Matthews, D. H. 1963. Magnetic anomalies over oceanic ridges. *Nature*, **199**, 947–9.
- Vine, F. J. and Wilson, J. T. 1965. Magnetic anomalies over a young oceanic ridge off Vancouver Island. *Science*, **150**, 485–9.
- White, R. and McKenzie, D. 1989. Magmatism at rift zones: the generation of volcanic continental margins and flood basalts. *J. Geophys. Res.*, **94**, 7685–729.
- Wilson, D. S., Hey, R. N., and Nishimura, C. 1984. Propagation as a mechanism of reorientation of the Juan de Fuca Ridge. *J. Geophys. Res.*, **89**, 9215–25.
- Zatman, S., Gordon, R. G. and Richards, M. A. 2001. Analytic models for the dynamics of diffuse oceanic plate boundaries. *Geophys. J. Int.*, **145**, 145–56.